A RESTRICTED FOUR-BODY MODEL FOR THE DYNAMICS NEAR THE LAGRANGIAN POINTS OF THE SUN-JUPITER SYSTEM

Frederic Gabern and Àngel Jorba

Departament de Matemàtica Aplicada i Anàlisi
Universitat de Barcelona
Gran Via 585, 08007 Barcelona, Spain
E-mails: gabern@mat.ub.es, angel@maia.ub.es

Abstract. We focus on the dynamics of a small particle near the Lagrangian points of the Sun-Jupiter system. To try to account for the effect of Saturn, we develop a specific model based on the computation of a true solution of the planar three-body problem for Sun, Jupiter and Saturn, close to the real motion of these three bodies. Then, we can write the equations of motion of a fourth infinitesimal particle moving under the attraction of these three masses. Using suitable coordinates, the model is written as a time-dependent perturbation of the well-known spatial Restricted Three-Body Problem.

Then, we study the dynamics of this model near the triangular points. The tools are based on computing, up to high order, suitable normal forms and first integrals. From these expansions, it is not difficult to derive approximations to invariant tori (of dimensions 2, 3 and 4) as well as bounds on the speed of diffusion on suitable domains. We have also included some comparisons with the motion of a few Trojan asteroids in the real Solar system.

1. Introduction

Let us start by introducing the well known Restricted Three Body Problem (from now on, RTBP). The RTBP models the motion of a particle under the gravitational attraction of Jupiter and Sun (also called primaries), under the following assumptions: i) the particle is so small that it does not affect the motion of Jupiter and Sun; and ii) Jupiter and Sun are point masses that revolve in circular orbits around their common centre of mass. It is usual to take a rotating reference frame with the origin at the centre of mass, and such that Sun and Jupiter are kept fixed on the x axis, the (x, y) plane is the plane of motion of the primaries, and the z axis is orthogonal to the (x, y) plane. These coordinates are sometimes called synodical. The usual (adimensional) units are chosen as follows: the unit of distance is the Sun–Jupiter distance, the unit of mass is the total Sun–Jupiter mass, and the unit of time is such that the period of Jupiter around the Sun equals 2π. With this selection of units, it turns out that the gravitational constant is also equal to 1. Defining momenta as $p_x = \dot{x} - y$, $p_y = \dot{y} + x$ and $p_z = \dot{z}$, the equations of motion for the particle can be written as an autonomous Hamiltonian system with three degrees of freedom. The corresponding Hamiltonian function is

$$H_{RTBP} = \frac{1}{2}(p_x^2 + p_y^2 + p_z^2) + yp_x - xp_y - \frac{1-\mu}{r_{PS}} - \frac{\mu}{r_{PJ}},$$

1991 *Mathematics Subject Classification.* 70F15, 65P40, 37J40.

Key words and phrases. Trojan asteroids, normal forms, first integrals, invariant tori.

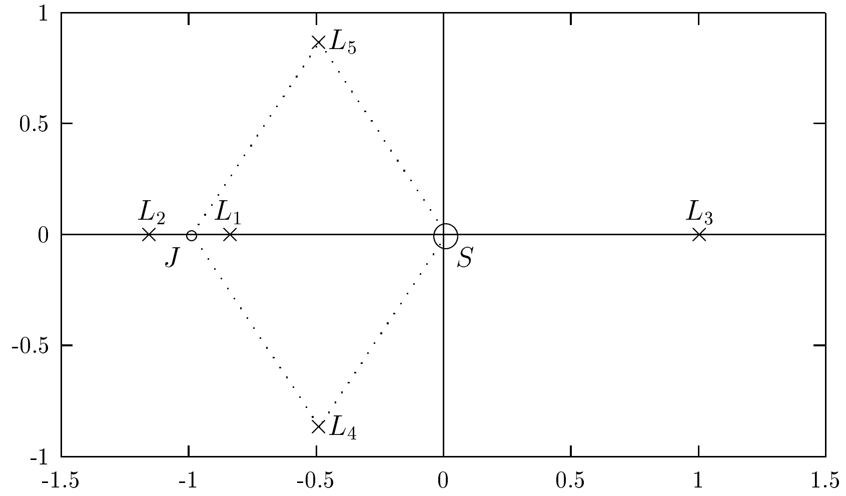

FIGURE 1. The five equilibrium points of the RTBP.

being μ the mass of Jupiter (in adimensional units), $r_{PS}^2 = (x-\mu)^2 + y^2 + z^2$ is the distance from the particle to the Sun, and $r_{PJ}^2 = (x-\mu+1)^2 + y^2 + z^2$ is the distance from the particle to Jupiter. The details can be found in almost any textbooks on Celestial Mechanics (for instance, see [43, 50]).

It is also well known that, in these –rotating– coordinates, the RTBP has five equilibrium points (see Figure 1): three of them lay on the x axis (they are called collinear points, Eulerian points, or simply $L_{1,2,3}$), and the other two form an equilateral triangle (in the (x, y) plane) with Sun and Jupiter (they are called triangular points, Lagrangian points or simply $L_{4,5}$).

It is not difficult to study the linear stability of these points. The collinear points are of the type centre×centre×saddle (for all μ), while the stability of the triangular points depends on the value of μ. If μ is lower than $\mu_R = \frac{1}{2}(1-\sqrt{23/27})$ (this value is known as the Routh mass, or Routh critical value), these points are linearly stable. On the contrary, for $\mu_R < \mu < \frac{1}{2}$, these points are unstable. The usual cases in the solar system (like Sun–Jupiter or Earth–Moon) have a mass parameter lower than μ_R, so they are linearly stable ([50]).

The nonlinear stability of elliptic points of conservative systems is a difficult problem. The case of two degrees of freedom is solved by the celebrated KAM theorem ([37, 3, 45], see [5] for a survey, or [8] for a presentation in a more general context), while the general case is still an open problem. On one side, a theorem by Lagrange and Dirichlet (see [5], p. 271) shows that, if the Hessian of the Hamiltonian function at the equilibrium point is positive definite, then the elliptic point is stable, in the classical Lyapunov sense. On the other hand, there is also a well-known example (see [16]) of a C^∞ –and not analytic– system with a linearly stable equilibrium point that is unstable for the complete system (see also [17] for the analytic case).

Under very general conditions, the KAM theorem can be applied to the neighbourhood of the Lagrangian points of the RTBP [38, 14, 41, 42, 44] to ensure the existence of many quasi-periodic motions. Each quasi-periodic trajectory fills densely a compact manifold diffeomorphic to a torus. The union of these invariant tori is a set with positive Lebesgue measure, and empty interior. In the planar case (the motion of the particle is restricted to the $z = p_z = 0$ plane, so the system only has two degrees of freedom), each torus is a two-dimensional manifold that separates the 3-D energy surface, so it acts as a confiner for the motion –this is the key point in the stability proof for two degrees of freedom Hamiltonian systems–. In the spatial case, the tori are now 3-D and the energy manifold is 5-D, so the tori cannot act as a barrier for the motion. Hence, it is possible to have trajectories that wander between these tori and escape from any vicinity of an elliptic point. The existence of such trajectories is believed to happen generically in non-integrable Hamiltonian systems. This phenomenon is known as Arnol'd diffusion since it was first conjectured by V.I. Arnol'd in [4].

A different approach to the stability of Hamiltonian systems was introduced by N.N. Nekhoroshev in [46]. The idea is to derive an upper bound on the diffusion velocity on an open domain of the phase space, and to show that the (possible) instability is so slow, that it does not show up in practical applications. This leads to the concept of effective stability of a given physical system: A system is considered effectively stable if the time needed to "observe" significant changes is longer than the expected lifetime of the system itself. For instance, [19] shows, among other things, the effective stability of a neighbourhood of the triangular points of the RTBP in the Sun-Jupiter case, for a time span of the order of the estimated age of the Solar system. Remarkable works in this direction are also [48, 10, 6]. For an application to a more general situation, see [47].

We can summarize both approaches by saying that KAM theory ensures true stability (i.e., for all times) on a set of initial conditions of large Lebesgue measure but with empty interior –this set is completely filled up with quasi-periodic motions– while Nekhoroshev theory ensures the effective stability (i.e., for a finite but very long time) of an open set of initial conditions. A formal presentation of these ideas in a more general setting can be found in [32].

A natural question is the persistence of these stability regions near the Lagrangian points of the Sun-Jupiter system in the real Solar system. With regard to this question it is remarkable that, in 1906, Max Wolf discovered (photographically) an asteroid (named 588 Achilles) moving near the Lagrangian point L_4 of the Sun-Jupiter system. Since then, many other asteroids have been found near the triangular points of the Sun-Jupiter system; they are usually called "Trojans", and the names of the most relevant ones have been chosen from the Iliad. These asteroids (or, at least, some of them) seem to move in a stable zone near the equilateral points. There have been many attempts to rigorously prove the stability of the motion of some of these asteroids in the RTBP, with little success (see Section 1.1). We note that, even if a proof of effective stability in the RTBP were available, the (effective) stability of the Trojan asteroids would still remain an open problem, since the RTBP is not an accurate model for the dynamics of an asteroid in the real Solar system (see Section 3.1).

One of the most accurate models for the dynamics of the Solar system is given by the so-called JPL ephemeris (see [36]). Essentially, this model is a computer file storing a sequence of interpolating polynomials for the position of all the planets; these polynomials have been derived from suitable numerical integrations of a very sophisticated model –it includes, for instance, relativistic corrections–. So, this is a numerical model, only defined for a limited time span –the longest version is only valid for 6,000 years–. Hence, it is not difficult to integrate numerically the motion of a particle in the JPL model, but it seems extremely difficult to derive theoretical results for such a complex model.

It seems then natural to look for a scaffolding of increasingly accurate (and increasingly complicated) models, starting at the RTBP and approaching the JPL model. In each of these models we focus on some dynamical structures that we study in detail. This detailed study of features of one model can be taken as the starting point of another study in the next model in our hierarchy of accuracy. At each stage new phenomena appear. At the end we uncover some phenomena present in the most realistic model but not present (even in a qualitative form) in the most simplified one. For an example of this technique see, for instance, [9] and [28].

There are several ways to introduce intermediate models, and we will summarize some of them in the following sections. One of the goals of this paper is to introduce an intermediate model, trying to take into account the effect of Saturn. This model is based on the numerical computation of a periodic orbit for the (non-restricted) three body problem Sun-Jupiter-Saturn, close to the (non periodic) orbit of these bodies in the real Solar system. Using this orbit, it is not difficult to write the equations of motion of a particle under the gravitational attraction of these bodies. In suitable coordinates, these equations are written as a periodic time-dependent perturbation of the RTBP, where the time-dependence accounts for the effect of Saturn. The remaining part of this work is focused on the study of this model. We have also included some comparisons with the real Solar system, by means of the JPL ephemeris [36].

The paper has been structured as follows: the remaining sections of the introduction are: Section 1.1, that describes previous results on the nonlinear stability of the triangular points of the RTBP; Section 1.2 that contains a description of models that include effects coming from perturbing bodies; and Section 1.3 summarizes the study and results obtained on the model presented here. Then, Section 2 describes the details on the derivation of the four-body model, Section 3 contains some numerical integrations comparing the model obtained with the RTBP and JPL model plus a numerical estimation of the stability region around the orbit. Section 4 deals with the preparation and initial expansion of the Hamiltonian of the restricted four-body problem, Section 5 is devoted to the computation of a normal form of order 16 around a periodic orbit near the triangular point, and to the computation of a region of effective stability around this orbit using estimates on the remainder of the normal form, Section 6 deals with the computation of formal first integrals (up to high order) and the use of these integrals to again estimate the stability region around the periodic orbit. The conclusions are presented in Section 7.

1.1. **The restricted three body problem.** As it has been explained before, this is the simplest model to study this problem. Hence, it has been used by several authors to try to show the stability of the Trojan asteroids for this model. The usual techniques are based in normal form calculations (see [19, 48]) or first integrals ([10]), but none of these works has been able to show the effective stability of a Trojan asteroid. The first stability calculation for a Trojan can be found in [21], although the authors use a planar model instead of a three-dimensional one. Hence, they show the stability for the projection, on the plane of motion of Jupiter, of the position of a real Trojan. Although [21] paper is strongly based on numerical calculations and for this reason cannot be regarded as a standard mathematical proof, it is, in our opinion, quite close to a rigorous computer-assisted proof.

1.1.1. *The elliptic restricted three body problem.* An improvement over the RTBP can be done by assuming that the two main bodies revolve not on a circular orbit but on an elliptic one. This is what is known as the elliptic RTBP (see [50]). In suitable coordinates, this model can be seen as a periodic time-dependent perturbation of the RTBP. The linearization of the flow around the triangular points of the RTBP model for the Sun-Jupiter case is described by the direct product of three linear oscillations, two of them are contained in the $z = p_z = 0$ plane and the third one is contained in the $x = p_x = y = p_y = 0$ plane. It is remarkable that the vertical oscillation has a frequency exactly equal to 1, for all the values of the mass parameter μ ([50]). This frequency 1 corresponds to a period of 2π that is also the period of revolution of the primaries in the synodic reference system. Hence, if we look at the effect of a small eccentricity on the motion of the primaries as a periodic time-dependent perturbation of the RTBP, then the period of this perturbation will be exactly 2π –the elliptic motion of the primaries is exactly repeated after one revolution–. In other words, we have an exact 1:1 resonance between one of the linear modes around $L_{4,5}$ of the RTBP and the perturbation coming from the eccentricity of Jupiter. However, this resonance does not play any role in the linearized system, since the perturbation is uncoupled –at first order– from the "vertical mode" with frequency 1. The linear dynamics near the Lagrangian points of the elliptic RTBP has been studied by several authors (see [13, 50]).

When one considers the nonlinear dynamics around the triangular points of the elliptic problem, the above-mentioned resonance becomes relevant, giving rise to hyperbolic, lower dimensional tori near the point. It is also worth to mention that these hyperbolic tori are not an obstruction to the existence of regions of effective stability. See [30] for more details.

1.2. **Restricted four-body models.** Now, to try to account for the effect of Saturn, we will introduce a four massive body into the model. As we will see, there are several ways of introducing the effect of such a body.

1.2.1. *The Bicircular model.* It was first introduced in [12] to include the effect of the Sun in the Earth–Moon RTBP. This model assumes that Earth and Moon are moving as in the RTBP, but also that the centre of mass of this RTBP is moving in a circular orbit around the Sun. The three bodies are assumed to move in the same plane. Then, once the motion of these three massive bodies has been prescribed (using very simple trigonometric expressions), it is not difficult to write the force acting on an infinitesimal particle and to derive the equations of motion for such a particle. It is usual to use the same reference frame as in the RTBP: the origin is taken at the Earth-Moon barycentre, with the same axis as in the RTBP. Hence, in these coordinates, the Sun is turning (clockwise) around the origin. For recent results on this model in the Earth-Moon case, see [24, 49, 29, 9, 28].

We can apply a similar approach to introduce the effect of Saturn into the model: we can assume that Sun and Jupiter move as in the RTBP, and that Saturn also moves in circular orbit around the Jupiter-Sun barycentre, and that the three bodies move in the same plane. Then, as in the Earth-Moon case, it is not difficult to derive the equations of motion of a fourth infinitesimal particle under the Newtonian attraction of these bodies. Defining momenta as $p_x = \dot{x} - y$, $p_y = \dot{y} + x$ and $p_z = z$, the Hamiltonian for this Bicircular model is given by

$$
\begin{aligned}
H &= \frac{1}{2}(p_x^2 + p_y^2 + p_z^2) + yp_x - xp_y - \\
&\quad -\frac{1-\mu}{r_s} - \frac{\mu}{r_j} - \frac{m_{sat}}{r_{sat}} - \frac{m_{sat}}{a^2}(y\sin(\theta - \theta_0) - x\cos(\theta - \theta_0)),
\end{aligned}
$$

where $r_s^2 = (x-\mu)^2 + y^2 + z^2$, $r_j^2 = (x - \mu + 1)^2 + y^2 + z^2$, $r_{sat}^2 = (x - x_{sat})^2 + (y - y_{sat})^2 + z^2$, $x_{sat} = a\cos(\theta - \theta_0)$, $y_{sat} = -a\sin(\theta - \theta_0)$, $\theta = \omega_{sat}t$, being m_{sat}, ω_{sat} and a the mass, frequency and semi-major axis of the orbit of Saturn, in the RTBP units.

1.2.2. *Coherent periodic models.* A characteristic of the Bicircular model is that the motion of the three massive bodies is not coherent, in the sense that they do not follow Newton's law. This lack of coherence is due to the selection of circular trajectories for the bodies, to avoid a too complex model.

To derive a coherent model, we need first to compute a true solution of the general Three Body Problem (from now on, TBP), close to the real motion of Sun, Jupiter and Saturn. Although this is already a difficult problem, it can be solved by means of numerical methods. Then, it is not difficult to write the equations of motion for a particle under the gravitational attraction of these three bodies. Finally, using a suitable change of coordinates –in which Sun and Jupiter are kept fixed on the x-axis, as in the RTBP–, these equations of motion are written as a periodic time-dependent perturbation of the RTBP. In what follows, we will refer to these kind of models as Bicircular Coherent Periodic Models or BCCP.

A coherent model for the Earth-Moon-Sun problem has been developed in [1, 2], to study the dynamics near the collinear points $L_{1,2}$ of the Earth-Moon system. Here we will focus on the Sun-Jupiter-Saturn case and, although we will roughly follow the methods developed in [1], we will also introduce a few changes to simplify the technicalities of the method.

1.2.3. *Quasi-periodic models.* Assume we are given a model for the motion of the bodies of the Solar system (for instance, the JPL ephemeris), and that we are interested in the dynamics near the triangular points of the Sun-Jupiter system. Then, we can proceed as follows:

a) Write the vector field acting on a particle under the gravitational attraction of all the planets.
b) Take coordinates (a time dependent reference frame) such that Sun and Jupiter are kept fixed on the x axis. As in the RTBP, we will refer to these coordinates as synodical. Write the vector field defined in a) in these coordinates.

Now we have a vector field that can be seen as a perturbation of the RTBP, but with more terms that depend on the transformation used –that is, of the real position of Sun and Jupiter– plus the position of the bodies of the Solar system. Note that these extra terms depend on the positions of Sun and planets and that, for a model like the JPL ephemeris, there are no "simple closed formulas" for them. Then, we can apply the following steps:

c) Perform a frequency analysis on these terms, and detect the dominant frequencies. As the motion of the Solar system seems to be quasi-periodic (at least for moderate time spans), it turns out that the part of these perturbing terms that depend on the positions of Sun and planets can be well approximated by Fourier series.

d) We substitute the dependence of the positions of the bodies by these truncated Fourier series.
e) The frequencies detected in c) can be written as a linear combination of a few of them, that correspond to the mean motion of the elements of the orbits of the bodies. We will refer to them as basic frequencies.
f) It is not necessary to take into account all the basic frequencies. In fact, the frequencies selected can be used as a control on the complexity (and the accuracy) of the model.

As far as we know, these models were first introduced in [25, 23, 24] (see also [26]) to apply dynamical systems tools to the transfer and control of space missions (see also [15, 22, 11]). Theoretical results for these kind of models can be found in [31] and [33].

1.3. **Study of the coherent periodic model.** We will focus on the dynamics near the Lagrangian point L_5. The same results will hold for L_4, due to the symmetries of the model.

1.3.1. *Periodic orbits as replacements of* $L_{4,5}$. Due to the effect of Saturn, the equilateral points are not longer equilibrium points. A simple application of the Implicit Function Theorem shows that, under generic hypotheses of non-resonance and smallness of the perturbation of Saturn, the equilibrium points of the RTBP are replaced by periodic orbits with the same frequency as the perturbation. These periodic orbits tend to the respective equilibrium points when the perturbation goes to zero.

The first step is to compute the periodic orbit that is replacing L_5, and to study its linear normal behaviour. This information will be used to compute an affine transformation that brings the Hamiltonian into linear normal form. We note that the case of a periodic orbit of an autonomous system is much more involved, since this transformation cannot be taken as affine, see [34] for more details.

1.3.2. *Normal forms and first integrals.* Next step is to compute a complete (and integrable) normal form around this orbit up to a high order (typically, we will use order 16). This means that we will expand the Hamiltonian in power series (of the 6 phase space coordinates) up to degree 16. Note that the coefficients of the corresponding monomials depend on time in a periodic way. Hence, we will handle them as truncated Fourier series with double precision coefficients. The truncation has been selected to only drop terms whose contribution is less than 10^{-16}, the truncation error of the computer arithmetic. We stress that we are using truncated formal Fourier-Taylor expansions for the Hamiltonian, but with double precision coefficients. The use of the standard floating point arithmetic instead of a symbolic (and exact) arithmetic allows huge savings both in memory and time for the programs. This, jointly with an efficient implementation of the algorithms, is the key that allows to reach order 16 in a standard PC.

The integrability of the normal form can be achieved since the frequencies ω_j ($j = 1, 2, 3$) and ω_{sat} have no exact resonances, at least up to order 16. Hence, it is possible to introduce action-angle variables such that the truncated normal form, to degree 16, only depends on the actions. Then, it is not difficult to describe approximately the dynamics around the periodic orbit. In a similar way it is possible to compute approximate first integrals, as a power expansion with periodic time-dependent coefficients. These functions (sometimes called "quasi integrals" [39]) can be used to derive estimates of the diffusion time near the orbit ([10, 20]).

The computational process is based on the use of generating functions and Lie series. The algorithm used for the normal form computation is a modification of the classical Lie series method (see [27] for the details of this modified method), to deal with periodic time-dependent Hamiltonian (see [24, 30, 49]). The main advantage of the method presented in [27] is to avoid dealing with the Lie triangle (it would require too much memory). These algorithms have been coded in C++ (C or FORTRAN would have also been a good choice), since the use of general purpose packages of algebraic manipulation requires a prohibitive amount of computer memory and time. The computer program is then an enlargement of the one presented in [27].

1.3.3. *Dynamical implications.* The normal form will provide two kinds of information. From one side, we can use it to compute invariant tori of dimensions ranging from 2 to 4; this will give a description of the kind of motions near the periodic orbit. On the other side, we can bound (numerically) the remainder of the normal form and produce estimates of the time needed by a particle (like an asteroid) to escape from a neighbourhood of that periodic orbit. We have also used the first integrals to derive the region of effective stability. For the comparison between the two approaches, see Section 7.

A more direct method to estimate the region of effective stability near the triangular points is by means of a direct numerical integration: given a sufficiently fine mesh of points, we use them as initial conditions for a very long numerical integration, to discard those points whose subsequent evolution is not confined near the Lagrangian points. The main advantage of a direct numerical simulation is that we obtain a quite realistic estimate of the size of the stability region, and the main inconveniences are that the number of initial conditions in the mesh grows exponentially with the dimension of the mesh, and that the integration time cannot be arbitrarily long. For these reasons, in the simulations of Section 3.2 we have restricted ourselves to a two dimensional mesh (so we have obtained a slice of the region) and the time span has been restricted to 10^6 years.

On the other hand, the estimation of the region by means of normal forms and/or first integrals is much less affected by the stability time or the dimension of the phase space, and the results can be converted in mathematical proofs, provided that the computations are done using an exact arithmetic, like the intervalar one. The main weakness of these methods is that the regions obtained are much smaller than the real region of effective stability.

2. The BCCP model

This section is devoted to the construction of the BCCP model. First, we compute a periodic solution of the planar three-body problem close to the Sun-Jupiter-Saturn case; then we will use this solution to derive the equations for the BCCP model as a perturbation of the RTBP. A BCCP model for the Sun-Earth-Moon system has already been constructed in [1, 2].

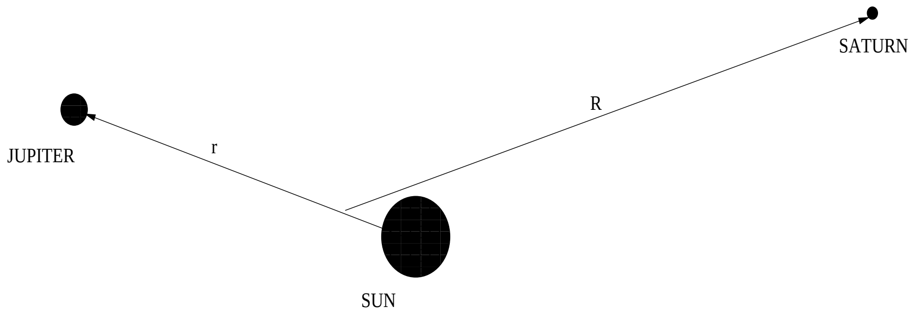

FIGURE 2. Jacobi coordinates for the TBP.

2.1. **A periodic solution of the general three-body problem.** Our first purpose is to obtain (numerically) a periodic solution of the planar three body problem (TBP). We will use the Jacobi formulation of the TBP, where we deal with two position vectors: one going from the Sun to Jupiter, and another one from the Sun-Jupiter barycentre to Saturn. This second vector contains the barycentre of the three masses (see Figure 2).

Taking units such that the total mass of Sun and Jupiter is equal to 1 and the gravitational constant is also 1, the equations of motion for the three massive bodies are (see [40]):

$$\begin{aligned} \ddot{\vec{r}} &= -\frac{\vec{r}}{r^3} + m_{sat}\left[\frac{\vec{R}-(1-\mu)\vec{r}}{|\vec{R}-(1-\mu)\vec{r}|^3} - \frac{\vec{R}+\mu\vec{r}}{|\vec{R}+\mu\vec{r}|^3}\right], \\ \ddot{\vec{R}} &= -(1+m_{sat})\left[\mu\frac{\vec{R}-(1-\mu)\vec{r}}{|\vec{R}-(1-\mu)\vec{r}|^3} + (1-\mu)\frac{\vec{R}+\mu\vec{r}}{|\vec{R}+\mu\vec{r}|^3}\right], \end{aligned} \tag{1}$$

where $\mu = 0.95387536 \times 10^{-3}$ and $m_{sat} = 0.285515017438987 \times 10^{-3}$. We will look for a solution in which the three bodies start on a line –Saturn, Jupiter and Sun, from left to right– and that they repeat this configuration (including speeds) after T units of time. Of course, the value of T has to be selected appropriately to obtain a solution as close as possible to the real motion of Sun, Jupiter and Saturn. Here, T is taken as the period of Saturn in the RTBP coordinates for the Sun-Jupiter system, assuming that both Jupiter and Saturn move on circular orbits. The associated frequency $\omega_{sat} = \frac{2\pi}{T}$ is then 0.597039074021947.

The procedure for the numerical computation of this periodic orbit is as follows: first, we apply the change of variables

$$\begin{aligned} r_x &= \xi_x\cos t - \xi_y \sin t, & R_x &= \eta_x \cos t - \eta_y \sin t, \\ r_y &= \xi_x \sin t + \xi_y \cos t, & R_y &= \eta_x \sin t + \eta_y \cos t, \end{aligned}$$

to equation (1). This is a uniform (counterclockwise) rotation with frequency 1, the frequency of Jupiter in the RTBP. Then, defining the momenta as usual,

$$\begin{aligned} p_x &= \dot{\xi_x} - \xi_y, & P_x &= \dot{\eta_x} - \eta_y, \\ p_y &= \dot{\xi_y} + \xi_x, & P_y &= \dot{\eta_y} + \eta_x, \end{aligned}$$

and renaming the variables ξ and η as r and R respectively (we hope the reader will not be confused by this), equations (1) become:

$$
\begin{aligned}
\dot{r_x} &= p_x + r_y, \\
\dot{r_y} &= p_y - r_x, \\
\dot{R_x} &= P_x + R_y, \\
\dot{R_y} &= P_y - R_x, \\
\dot{p_x} &= p_y - \frac{r_x}{r^3} - \frac{m_{sat}}{r^3_{Ssat}}(R_x + \mu r_x) + \frac{m_{sat}}{r^3_{Jsat}}(R_x - (1-\mu)r_x), \\
\dot{p_y} &= -p_x - \frac{r_y}{r^3} - \frac{m_{sat}}{r^3_{Ssat}}(R_y + \mu r_y) + \frac{m_{sat}}{r^3_{Jsat}}(R_y - (1-\mu)r_y), \\
\dot{P_x} &= P_y - (1+m_{sat})\left[\frac{1-\mu}{r^3_{Ssat}}(R_x + \mu r_x) + \frac{\mu}{r^3_{Jsat}}(R_x - (1-\mu)r_x)\right], \\
\dot{P_y} &= -P_x - (1+m_{sat})\left[\frac{1-\mu}{r^3_{Ssat}}(R_y + \mu r_y) + \frac{\mu}{r^3_{Jsat}}(R_y - (1-\mu)r_y)\right],
\end{aligned}
$$

where $r^2 = r_x^2 + r_y^2$, $r^2_{Ssat} = (R_x + \mu r_x)^2 + (R_y + \mu r_y)^2$ and $r^2_{Jsat} = (R_x - (1-\mu)r_x)^2 + (R_y - (1-\mu)r_y)^2$. The numerical computation of the periodic orbit is done by means of a Newton method, looking for an initial condition such that the vectors $\vec{r}$, $\vec{R}$ (see Figure 2) and their derivatives are periodic with period T. The initial conditions are kept on the x axis, so the bodies are always on the same line at the beginning of the orbit. We have also used a continuation scheme on the masses starting with $\mu = m_{sat} = 0$ (where the solution can be easily found by hand).

Let us describe this periodic solution. In an inertial frame, Jupiter and Saturn are turning counterclockwise. In the rotating frame, Jupiter is librating around the point $(\mu-1, 0)$ while Saturn is turning clockwise (see Figure 3). A more geometrical view can be obtained by computing, for each instant of time, the orbital elements of the orbits of Jupiter and Saturn: Figure 4 displays the variation of the instantaneous eccentricity and argument of the perihelion along a period. As the eccentricities are very small (the eccentricities of Jupiter and Saturn in the real Solar system are 0.048 and 0.054, respectively), we can conclude that the motion of Jupiter and Saturn around the Sun is very close to circular. Moreover, the averaged Sun-Saturn distance for this solution (1.8333) is very close to the real one (1.8315, in RTBP units).

Finally, we note that there are other options for the construction of the BCCP. Here we have used the synodic frequency of Saturn as a reference for selecting the periodic orbit of the TBP, but it is possible to use other elements of Saturn as a reference (for instance, its mean distance to the Sun). The differences between the results of these selections are very small.

2.2. The Hamiltonian of the BCCP model.

Here we will derive the equations of motion of a fourth massless particle under the attraction of the three primaries moving in the periodic orbit found in the previous section. One of the main goals is to write the model as a periodic time-dependent perturbation of the Sun-Jupiter RTBP.

We start from the periodic solution for Sun, Jupiter and Saturn, written in an inertial reference system, and let $\vec{\rho}$ be the position vector of the particle in this

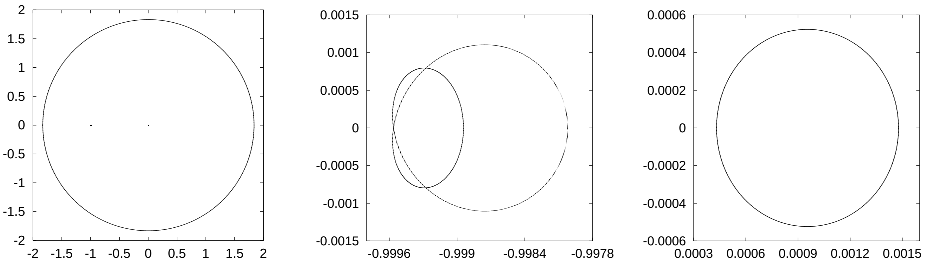

FIGURE 3. Periodic orbits of, respectively, Saturn, Jupiter and the Sun in the rotating reference frame. In fact, the plots for Jupiter and Sun are also displayed in Saturn's plot; they are seen as two small dots inside Saturn's orbit.

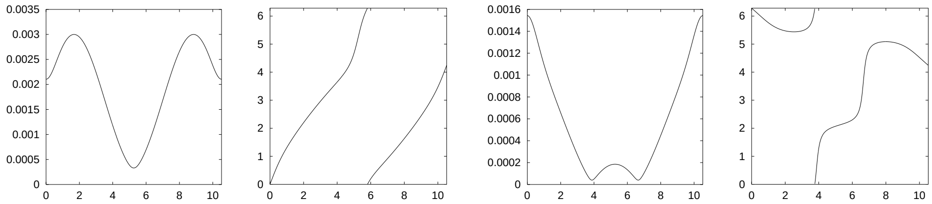

FIGURE 4. Orbital elements of Jupiter and Saturn for a full period of the BCCP. They correspond, from left to right, to the eccentricity and the perihelion argument of Jupiter (first and second plot) and Saturn (third and fourth plot).

inertial reference frame. We are going to use the change of variables obtained from the composition of the following three transformations.

a) Translation of the origin from the global barycentre to the Sun-Jupiter barycentre.
b) Periodic time-dependent rotation to fix Sun and Jupiter on the x-axis.
c) Scaling to force the distance between Sun and Jupiter to be one.

In this "rotating-pulsating" reference frame, the three main bodies and the particle have the coordinates:

$$\begin{aligned} S &: \vec{Q}_s = (\mu, 0, 0)^t \\ J &: \vec{Q}_j = (\mu - 1, 0, 0)^t \\ sat &: \vec{Q}_{sat} = \frac{1}{r} C^T \vec{R} \\ part &: \vec{q} = \frac{1}{r} C^t (\vec{\rho} + \frac{m_{sat}}{1 + m_{sat}} \vec{R}) \end{aligned}$$

where S, J, sat and $part$ stands for Sun, Jupiter, Saturn and particle, respectively, and $r = \|\vec{r}\|$ (note that $\vec{r}$ and $\vec{R}$ depend periodically on time). The matrix C is defined as

$$C = \begin{pmatrix} -\frac{r_x}{r} & \frac{r_y}{r} & 0 \\ -\frac{r_y}{r} & -\frac{r_x}{r} & 0 \\ 0 & 0 & 1 \end{pmatrix}$$

where $\vec{r} = (r_x, r_y, 0)$ and $\vec{R} = (R_x, R_y, 0)$ are the periodic solution of the TBP embedded in the three dimensional space. The inverse change is given by

$$\vec{\rho} = -\frac{m_{sat}}{1+m_{sat}}\vec{R} + B\vec{q},$$

where $B = rC$. Defining the conjugate momentum as

$$\vec{p} = r^2\dot{\vec{q}} + B^t\dot{B}\vec{q},$$

the equations for the particle become Hamiltonian, and the Hamiltonian is:

$$H = \frac{1}{2r^2}\langle\vec{p},\vec{p}\rangle - \frac{1}{r^2}\vec{p}B^t\dot{B}\vec{q} - \frac{m_{sat}}{1+m_{sat}}\ddot{\vec{R}}^t B\vec{q} + U,$$

where U, the potential energy, is given by

$$U = -\frac{1-\mu}{r||\vec{Q}_s - \vec{q}||} - \frac{\mu}{r||\vec{Q}_j - \vec{q}||} - \frac{m_{sat}}{r||\vec{Q}_{sat} - \vec{q}||}.$$

To write the Hamiltonian in a more suitable way, we look at the vectors $\vec{r}$ and $\vec{R}$ as if they were in the complex plane

$$\begin{aligned} z &= r_x + ir_y, \\ Z &= R_x + iR_y, \end{aligned}$$

and we define the (T-periodic) functions:

$$\begin{aligned}
\alpha_1 &= \frac{1}{r^2}, & \alpha_2 &= \frac{\mathrm{Re}\,(\dot{z}\bar{z})}{r^2}, & \alpha_3 &= \frac{\mathrm{Im}\,(\dot{z}\bar{z})}{r^2}, \\
\alpha_4 &= \frac{m_{sat}}{1+m_{sat}}\mathrm{Re}\,(\ddot{Z}\bar{z}), & \alpha_5 &= \frac{m_{sat}}{1+m_{sat}}\mathrm{Im}\,(\ddot{Z}\bar{z}), & \alpha_6 &= \frac{1}{r}, \\
\alpha_7 &= -\frac{1}{r^2}\mathrm{Re}\,(Z\bar{z}), & \alpha_8 &= -\tfrac{1}{r^2}\mathrm{Im}\,(Z\bar{z}).
\end{aligned}$$

From a numerical tabulation of the values of $\vec{r}$ and $\vec{R}$ we can easily compute the Fourier coefficients for α_j, $j = 1, \dots, 8$, up to a finite order (in fact, all the coefficients with modulus larger than 10^{-13} have been kept). Due to the parity properties of these functions, we can write them as

$$\begin{aligned}
\alpha_j(t) &= \sum_{k\geq 0}\alpha_{jk}\cos(k\omega_{sat}t), \qquad j = 1,3,4,6,7 \\
\alpha_j(t) &= \sum_{k\geq 1}\alpha_{jk}\sin(k\omega_{sat}t), \qquad j = 2,5,8
\end{aligned}$$

It is then possible to write the Hamiltonian of the BCCP problem as:

$$\begin{aligned}
H &= \frac{1}{2}\alpha_1(t)(p_x^2 + p_y^2 + p_z^2) + \alpha_2(t)(xp_x + yp_y + zp_z) + \alpha_3(t)(yp_x - xp_y) \\
&\quad + \alpha_4(t)x + \alpha_5(t)y - \alpha_6(t)\left[\frac{1-\mu}{q_S} + \frac{\mu}{q_J} + \frac{m_{sat}}{q_{sat}}\right], \qquad (2)
\end{aligned}$$

where $q_S^2 = (x-\mu)^2 + y^2 + z^2$, $q_J^2 = (x-\mu+1)^2 + y^2 + z^2$ and $q_{sat}^2 = (x-\alpha_7(t))^2 + (y-\alpha_8(t))^2 + z^2$. We recall that, for $t = 0$, Saturn is on the negative part of the x axis. Due to the symmetries of the periodic solution of the TBP, this Hamiltonian has the symmetry $(t, x, y, z, \dot{x}, \dot{y}, \dot{z}) \mapsto (-t, x, -y, z, -\dot{x}, \dot{y}, -\dot{z})$. This implies that, to study the triangular points, it is enough to focus on one of them.

We want to make some comparisons between the derivation of the BCCP done here and the method used in [1, 2] to compute a similar model for the Sun-Earth-Moon case. There, the authors compute the periodic solution of the TBP by means of an (specially built) algebraic manipulator to find a Fourier series that satisfies, up to a prescribed order, equation (1). Then, this truncated Fourier series is manipulated to obtain the functions α_j, $j = 1, \ldots, 8$.

The concrete values for the coefficients of the functions α_j, $j = 1, \ldots, 8$ can be obtained from `http://www.maia.ub.es/dsg/`, in the preprints section.

2.3. **Tests on the software.** To check the results obtained in the preceding calculations, we have compared numerical integrations of the obtained model (2) with a restricted four body problem: we have randomly selected initial conditions for the particle, and we have computed the subsequent orbit for a period of Saturn. Then, each of these orbits has been sent to the initial coordinates of the Jacobi formulation (1). Finally, adding the equation of the infinitesimal particle to (1), using the initial condition for the periodic orbit of the TBP and integrating the four particles at once, it is not difficult to test the accuracy of the initial orbit. We note that this not only tests the equations obtained, but also the changes of coordinates used. The differences between the two integrations are of the order of 10^{-12}. We note that, in the computation of the Fourier coefficients of the functions α_j we discarded all the coefficients whose absolute value is lower than 10^{-13}.

3. Numerical simulations

Here we have included some numerical simulations for the BCCP model, as well as some comparisons with the results for the RTBP and the JPL model for the real Solar system.

3.1. **Trajectories of some Trojan asteroids.** To compare the accuracies of the models RTBP and BCCP against the JPL ephemeris, we have integrated numerically the motion of the Trojan asteroids 588 Achilles and 624 Hektor (both are near L_4) and 1870 Glaukos (near L_5), in these three models. We have selected Achilles and Hektor because they are two well-known members of the Trojan family, and Glaukos because is one of the four Trojans whose effective stability has been shown in [21], but for the planar RTBP. The initial conditions have been taken at December 22nd, 2000 (i.e., Julian day 2451900.5), from the database [7], and the total integration time has been chosen to be 20 years –enough for our actual purposes–. Of course, for the integration in the BCCP we need to take into account the initial position of Saturn with respect to Jupiter, to select the right initial phase for the time variable. The results are displayed in Figures 5, 6 and 7.

Let us comment on these plots. First, note the proximity between the RTBP and the BCCP integrations. In fact, this is not surprising because of the construction of the BCCP: among all the solutions of the TBP, we have selected the simplest one, in the sense that the motion of Jupiter and Saturn is nearly circular. So, if we look at the gravitational forces acting on the asteroid in the RTBP and BCCP models, we see that the force coming from Jupiter is very similar for the two models, and the main difference is the effect of Saturn, which is small since it is far away. Note that, in the real system, Saturn has little effect on the asteroid but it has a strong effect on Jupiter. In other words, the main difference –we are looking at the forces acting on the asteroid– between RTBP and the real system is the different

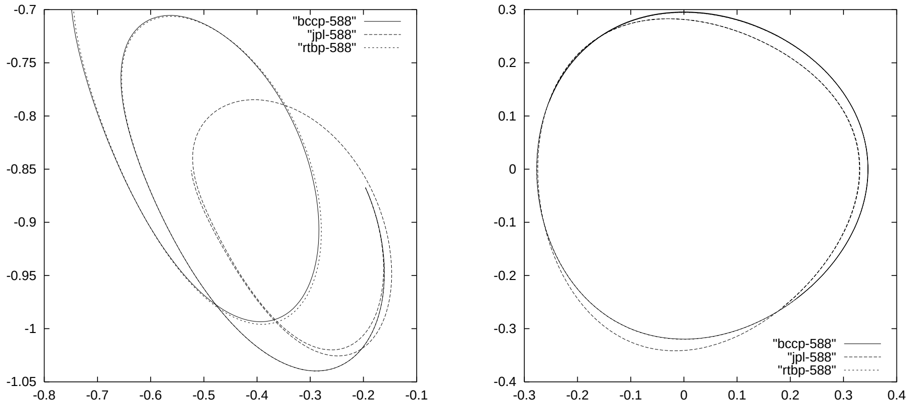

FIGURE 5. (x, y) and $(z, \dot{z})$ projections of the orbit of 588 Achilles for the RTBP, BCCP and JPL models, during 20 years.

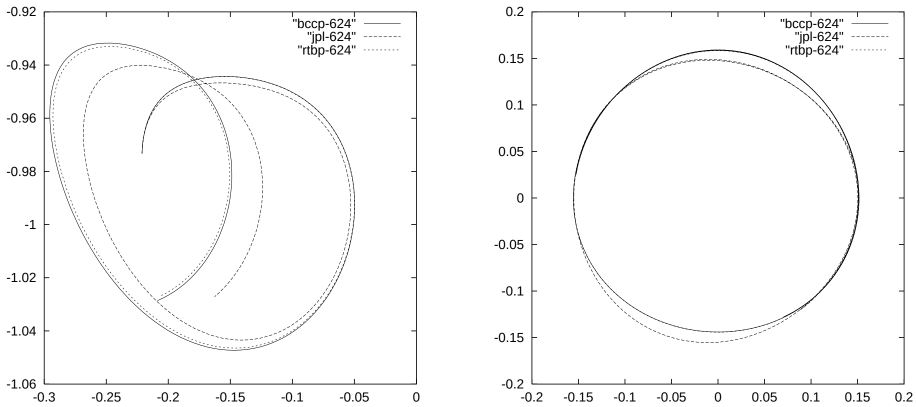

FIGURE 6. (x, y) and $(z, \dot{z})$ projections of the orbit of 624 Hektor for the RTBP, BCCP and JPL models, during 20 years.

motion of Jupiter. The main point in constructing the BCCP by introducing Saturn is to take into account the effect of Saturn on the orbit of Jupiter and, in second place, to account for the less important effect of Saturn on the asteroid. As we have explained, our particular –and simple– selection of solution for the TBP is not close enough to the motion of Jupiter in the real system. Hence, a natural improvement to the BCCP model is to look for a solution (of the TBP) not periodic but quasi-periodic, in which the motion of Jupiter is closer to the real one. This is actually work in progress.

Although, from these considerations, it could seem that the BCCP is so close to the RTBP that it is not worth to study, we think that the BCCP contains very interesting features. One of the most important is that, as the equilibrium point is replaced by a periodic orbit (see Section 4.1), the stability region is not located around the geometrical triangular point but it moves along the periodic orbit. As we will see in the following sections, this motion is wide enough such that we can show effective stability for points in the space that are outside of previously

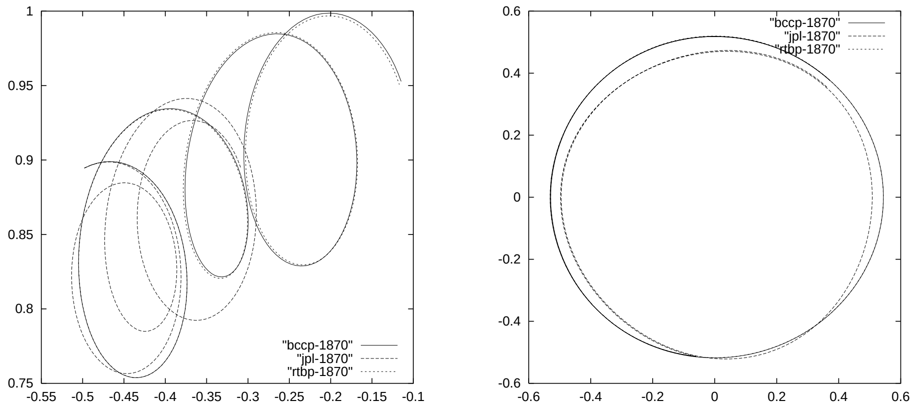

FIGURE 7. (x, y) and $(z, \dot{z})$ projections of the orbit of 1870 Glaukos for the RTBP, BCCP and JPL models, during 20 years.

computed regions for the RTBP. Of course, these points are inside these regions only for certain times (i.e., for certain positions of Saturn). See Section 7 for more details.

Finally, as a side comment, we want to note the simplicity of the $(z, \dot{z})$ projection of the motion: it looks like a mildly perturbed linear oscillator. This can be already explained using the RTBP: the linearization of the flow around L_5 in synodical coordinates contains a linear oscillator (of frequency 1) fully contained in the $(z, \dot{z})$ direction. When we take into consideration the nonlinear terms, we see that they have little influence in the vertical direction so the dynamics in this $(z, \dot{z})$ direction is close to an harmonic oscillator. Hence, for the full Solar system, we expect to have a similar behaviour.

3.2. **Numerical estimation of a stability region.** Figure 8 contains an estimation of the stability region of the BCCP for $t = 0$. This region has been obtained by the following procedure: a) selecting a grid of values (x, y) and taking the remaining coordinates from the position of the periodic orbit that substitutes L_5 (see Section 4.1) at time $t = 0$; b) using the previous values as initial conditions, we start a numerical integration of the BCCP model; and c) the trajectories that go away before the final integration time (10^6 years) are discarded. Hence, in Figure 8 we have drawn a black dot for each couple (x, y) giving rise to a trajectory that stays near the Lagrangian points for 10^6 years. The explored area is also displayed, enclosed with a semi-circular box. Of course, we can compute a similar region for each value of t along a period of Saturn in the BCCP coordinates.

We note the big size of the region (we recall that the unit of distance is the Sun-Jupiter distance). In the following sections, we will also obtain regions of effective stability using truncated normal forms and approximated first integrals. These regions will be much smaller than the one obtained here, as it is usual for this kind of computations.

4. PRELIMINARY TRANSFORMATIONS AND EXPANSIONS

Before starting with the normal form or first integral computations, we will put the initial Hamiltonian (2) into a more suitable form. First, we compute the

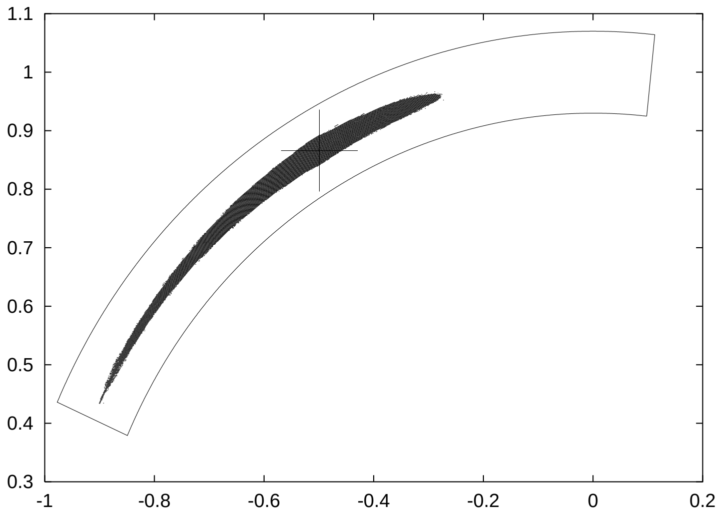

FIGURE 8. Numerical estimation of the stability region for the BCCP, for $t = 0$. The axis are the x and y synodical coordinates.

periodic orbit that replaces the equilibrium point L_5, since the (time-dependent) translation of the origin of coordinates to this orbit cancels the first order terms in the Hamiltonian. Then, we will compute the linear transformation that reduces the linear variational equations along the orbit to constant coefficients. This (canonical) transformation reduces the second degree terms in the Hamiltonian to constant coefficients. Moreover, this reducing transformation can be taken such that the Hamiltonian is put in (complex) normal form up to second degree. Finally, we will expand, up to high order, the Hamiltonian in these coordinates. The resulting expansion will be used in Sections 5 and 6. This procedure has already been used in [24, 30].

4.1. **The periodic orbit that replaces L_5.** As it has been mentioned before, the equilibrium points of the RTBP are no longer equilibrium solutions for the BCCP. A straightforward application of the Implicit Function Theorem shows that, under suitable conditions (essentially, they are a non-resonance condition involving the perturbing frequencies and the linear modes around the point, and a smallness condition on the size of the perturbation), the equilibrium points are replaced with periodic orbits with the same period as the perturbation; these orbits go to the corresponding point when the perturbation goes to zero.

To compute this periodic orbit, we will consider the time period-of-Saturn map associated to the flow of the BCCP, and we will look for a fixed point. Note that this map can be easily evaluated by numerical integration of the flow associated to (2), and its differential is also obtained integrating the variational flow. Hence, it is not difficult to apply a Newton method to look for a fixed point. Due to the smallness of the perturbation, it is enough to use, as initial condition, the coordinates of the triangular point L_5. The (x, y) projection of the resulting periodic orbit is shown in Figure 9.

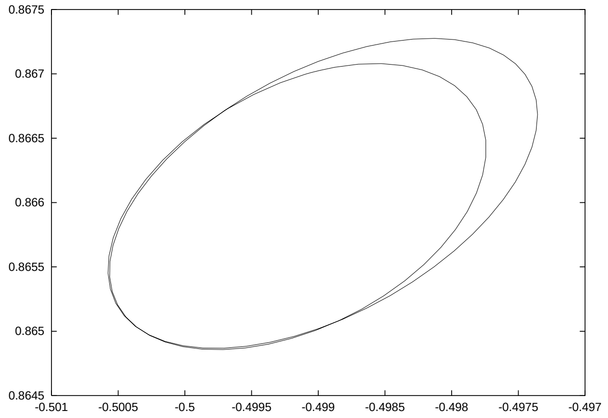

FIGURE 9. (x, y)-projection of the periodic orbit near L_5

j	$\mathrm{Re}\,(\lambda_j)$	$\pm\mathrm{Im}\,(\lambda_j)$	$\lvert\lambda_j\rvert$	$\pm\mathrm{Arg}\,(\lambda_j)$
1	0.662312812634	0.749227427569	1.0	0.846894831435
2	-0.485147270414	0.874432459375	1.0	2.077327904892
3	-0.453737377106	0.891135451330	1.0	2.041751159215

TABLE 1. Eigenvalues of the monodromy matrix of the periodic orbit near L_5.

To check for possible bifurcations of this orbit when the size of the perturbation increases from zero to its actual value, we have introduced a perturbing parameter in the Hamiltonian of the BCCP,

$$\begin{aligned} H_\varepsilon &= \frac{1}{2}(1+\varepsilon(\alpha_1(t)-1))(p_x^2+p_y^2+p_z^2)+\varepsilon\alpha_2(t)(xp_x+yp_y+zp_z) \\ &\quad +(1+\varepsilon(\alpha_3(t)-1))(yp_x-xp_y)+\varepsilon\alpha_4(t)x+\varepsilon\alpha_5(t)y \\ &\quad -(1+\varepsilon(\alpha_6(t)-1))\left[\frac{1-\mu}{q_S}+\frac{\mu}{q_J}\right]-\varepsilon\alpha_6(t)\frac{m_{sat}}{q_{sat}}. \end{aligned}$$

Hence, $\varepsilon = 0$ corresponds to the RTBP, while $\varepsilon = 1$ corresponds to the BCCP. By means of a continuation procedure, we have computed the periodic orbit for ε ranging from 0 to 1, showing a continuous behaviour of the periodic orbit w.r.t. ε. We note that this is not the case in similar models (with a larger perturbation), like the Bicircular problem for the Sun-Earth-Moon system (see [49, 9]).

The linearized normal behaviour is given by the eigenvalues of the monodromy matrix of the periodic orbits, shown in Table 1. As these eigenvalues have modulus 1, the orbit is linearly stable.

4.2. **Second order normal form.** In the previous section we have derived a time-dependent translation that cancels the first order terms in the Hamiltonian. Here we will derive a linear change of variables (that depends on time in a periodic way) that puts the second degree terms of the Hamiltonian into a more convenient form. This is, essentially, the Floquet transformation for the variational flow along the periodic orbit, but taking into account the symplectic structure of the problem.

To simplify further steps in the normalizing process, we also apply a complexifying change of variables that put the second degree terms of the Hamiltonian in the so-called diagonal form.

4.2.1. *Implementation of the Floquet change.* The linear flow around the periodic orbit that replaces L_5 is described by a linear system of differential equations, that depends periodically on time, with period T,

$$\dot{u} = Q(t)u. \tag{3}$$

Our goal is to find a symplectic and T-periodic change of variables, $u = P(t)v$, such that $P(t)^{-1}(Q(t)P(t) - \dot{P}(t)) \equiv A$ does not depend on time. Then, using this transformation, (3) becomes autonomous:

$$\dot{v} = Av.$$

The existence of such a change is ensured by the classical Floquet theorem. Here, as we want to work not with the flow but with the Hamiltonian, we want this transformation to be canonical.

The construction of the transformation $P(t)$ as well as of the reduced matrix A follows from the proof of the Floquet theorem. Here we will give the details of the calculation of $P(t)$ and A for the BCCP case. In what follows we will denote by J the matrix of the standard symplectic form of $\mathbb{R}^6$,

$$J = \begin{pmatrix} 0 & I \\ -I & 0 \end{pmatrix},$$

where I stands for the 3×3 identity matrix. We note that, with this definition of J, the first three coordinates (of $\mathbb{R}^6$) correspond to the positions while the last three are the momenta.

We start with the computation of the monodromy matrix M of (3), by integrating the fundamental matrix over a period T. In this case, all the eigenvalues of this matrix are different and of modulus 1, so M can be reduced to diagonal form $D_M = \mathrm{diag}(\lambda_1, \lambda_2, \lambda_3, \overline{\lambda}_1, \overline{\lambda}_2, \overline{\lambda}_3)$. Let S be the diagonalizing transformation, $M = SD_MS^{-1}$ (due to the Hamiltonian structure of the problem, the columns of S can be scaled such that $S^tJS = -iJ$; this makes easier the computation of the inverse of S, $S^{-1} = -iJS^tJ$). Next, we can compute values ω_j, $j = 1, 2, 3$, such that $\lambda_j = \exp(i\omega_jT)$. Note that these values are not uniquely defined: if ω_j is one of them, then any of the values $\pm(\omega_j + \frac{2k\pi}{T})$, $\forall\, k \in \mathbb{Z}$, is also admissible. Here, we have selected the values of k and the sign such that the values $\pm(\omega_j + \frac{2k\pi}{T})$ are as close as possible to the frequencies of the (unperturbed) RTBP. This is the natural selection from a perturbative point of view, since the matrix $P(t)$ is then close to the identity. So, defining $D_B = \mathrm{diag}(i\omega_1, i\omega_2, i\omega_3, -i\omega_1, -i\omega_2, -i\omega_3)$ and $B = SD_BS^{-1}$, we have that B is a real matrix such that $M = \exp(BT)$. Then, it is not difficult to check that the matrix $P(t)$ that solves the initial value problem,

$$\dot{P}(t) = Q(t)P(t) - P(t)B, \qquad P(0) = I,$$

is a T-periodic transformation that brings (3) into the reduced form $\dot{v} = Bv$.

Therefore, we have derived constructively the existence of the reducing transformation. However, we will first introduce a small modification on the scheme above to obtain a simpler reduced matrix B, and we then discuss the canonical character of the transformation $u = P(t)v$.

We want to compute a real transformation R such that $A = R^{-1}BR$ have a very simple form. Hence, we define R as the matrix whose first three columns are the real parts of the eigenvectors of M, and the last three columns are the corresponding imaginary parts (as before, due to the Hamiltonian structure of the problem, it is possible to scale the columns of R such that R becomes symplectic, $R^tJR = J$, and then the computation of R^{-1} becomes trivial). Then, it can be checked that the matrix $A = R^{-1}BR$ takes the form

$$A = \left(\begin{array}{ccc|ccc} 0 & 0 & 0 & \omega_1 & 0 & 0 \\ 0 & 0 & 0 & 0 & \omega_2 & 0 \\ 0 & 0 & 0 & 0 & 0 & \omega_3 \\ \hline -\omega_1 & 0 & 0 & 0 & 0 & 0 \\ 0 & -\omega_2 & 0 & 0 & 0 & 0 \\ 0 & 0 & -\omega_3 & 0 & 0 & 0 \end{array}\right).$$

Finally, it is not difficult to see that the solution of the initial value problem,

$$\dot{P}(t) = Q(t)P(t) - P(t)A, \qquad P(0) = R,$$

is a T-periodic matrix that reduces (3) to

$$\dot{v} = Av.$$

Finally, to ensure that the transformation is canonical, we only need to check that $P(t)$ is a symplectic matrix. This can be proved analytically (see [24]) but here, to also check the correctness of the software, we have tested numerically this condition for a mesh of values of t, with good agreement.

We also want to note that the selection of sign for the ω_j plays an essential role in the canonical character of the transformation. For instance, changing the sign of one of the ω_j when computing the logarithm of the monodromy matrix would end up in a non-symplectic matrix $P(t)$. If the reader is not familiar with these properties, we recommend the papers [19], [48] or [27] for a similar discussion for an autonomous system (as the Hamiltonian considered in these papers is simpler and the calculations can be carried out by hand, the discussion is probably much clearer).

Implementing this (time depending) change of variables, the second degree terms of the Hamiltonian become:

$$H_2 = \frac{1}{2}\omega_1(x_1^2 + y_1^2) + \frac{1}{2}\omega_2(x_2^2 + y_2^2) + \frac{1}{2}\omega_3(x_3^2 + y_3^2), \tag{4}$$

where the frequencies are $\omega_1 = -0.08047340341466$, $\omega_2 = 0.99668687782956$ and $\omega_3 = 1.00006744139040$. Due to the different signs for the values of the ω_j, the Hessian of H_2 is not positive definite. Hence, we cannot use the Lagrange-Dirichlet theorem to derive the nonlinear stability of the periodic orbit that replaces L_5.

4.2.2. *Complexification.* To simplify the subsequent steps in the normalizing process, it is very convenient to bring (4) into diagonal form. This can be achieved by means of a complexifying change of variables,

$$x_j = \frac{q_j + ip_j}{\sqrt{2}}, \quad y_j = \frac{iq_j + p_j}{\sqrt{2}}, \quad j = 1, 2, 3. \tag{5}$$

It is trivial to check that this defines a symplectic transformation that casts (4) into the form:

$$H_2 = i\omega_1 q_1 p_1 + i\omega_2 q_2 p_2 + i\omega_3 q_3 p_3. \tag{6}$$

This complexification is composed with the above-defined real matrix $P(t)$, to produce a (now complex) transformation, $P_c(t)$, that puts the second degree terms of the Hamiltonian into the form (6).

4.3. **Expansion of the Hamiltonian.** We need to produce a power expansion of the Hamiltonian (2), in the complex coordinates described before,

$$H = \sum_{n=2}^{N} H_n(q,p,\theta) + R_{N+1}(q,p,\theta),$$

where H_n, $n \geq 2$, denotes an homogeneous polynomial of degree n in the variables q and p, and H_2 is (6). To describe how to produce such expansion, we focus first on the terms

$$\frac{1}{s_l} = \frac{1}{\sqrt{(x - x_l(\theta))^2 + (y - y_l(\theta))^2 + z^2}}, \tag{7}$$

where l stands for S (the Sun), J (Jupiter) or sat (Saturn). If we write

$$\frac{1}{s_l} = \sum_{n \geq 0} A_n^l(x,y,z,\theta),$$

where A_n^l denotes an homogeneous polynomial of degree n whose coefficients are 2π periodic functions of θ. The expressions A_n^l can be easily written in terms of the Legendre polynomials, as it is explained in [27] (see also [30]). Then, the recurrence of the Legendre polynomials allows to prove that

$$A_{n+1}^l = \frac{1}{x_l^2(\theta) + y_l^2(\theta)} \left[\frac{2n+1}{n+1}(x_l(\theta)x + y_l(\theta)y)A_n^l - \frac{n}{n+1}(x^2+y^2+z^2)A_{n-1}^l \right],$$

for $n \geq 1$. The recurrence can be started using the values

$$A_0^l = \frac{1}{\sqrt{x_l^2(\theta) + y_l^2(\theta)}}, \qquad A_1^l = \frac{x_l(\theta)x + y_l(\theta)y}{(x_l^2(\theta) + y_l^2(\theta))^{3/2}}.$$

As the derivation of these formulas is a straightforward modification of the autonomous case (explained in [27]), we are convinced that the interested reader will not have any difficulty in proving them.

Now, the process to obtain the desired expansion for the Hamiltonian is the following. We first apply the translation that puts the periodic orbit that replaces L_5 at the origin. For simplicity, we call again to the new coordinates x, y, and z. After this translation, the terms $\frac{1}{s_l}$ still have the form (7). Next, we substitute the values of the variables x, y and z in the A_n^l, $n \geq 0$, by their expressions in terms of the variables q and p used in (6) –these expressions are given by the Floquet transformation $P_c(t)$ obtained before–. Then, we use the recurrence for the A_n^l up to a given degree $n = N$. In this way, we produce the expansion for the terms $\frac{1}{s_l}$ directly in the coordinates q, p (note that expanding first in the (x,y,z) coordinates and then substituting the Floquet transformation in this expansion requires much more work). Once the expansions for the three terms $\frac{1}{s_l}$ ($l = S, J, sat$) are obtained, we only need to insert these transformations in the remaining terms of (2). Due to the simplicity of these terms –they are all of second degree–, this insertion is done directly. Finally, once all these operations have been finished, we can check that we have obtained a power expansion, with periodic time-dependent coefficients, starting at degree two, in coordinates such that the second degree terms have the diagonal form (6).

4.4. **Bounds on the expansion.** Here we will include two lemmas that will be used later to estimate the size of the truncated terms in the expansion. To simplify the notation, we will denote by m_l the masses of the three bodies: $m_S = 1-\mu$ (Sun), $m_J = \mu$ (Jupiter), and m_{sat} (Saturn).

4.4.1. *Norms.* Let $f_n(u,v,\theta)$ be an homogeneous polynomial of degree n in the variables $(u,v) = (u_1,u_2,u_3,v_1,v_2,v_3)$, with periodic time-dependent coefficients,

$$f_n(u,v,\theta) = \sum_{|k|=n} \sum_{j\in\mathbb{Z}} f_{n,j}^k e^{ij\theta} u^{k^1} v^{k^2}, \quad k=(k^1,k^2)\in\mathbb{Z}^3\times\mathbb{Z}^3, \quad f_{n,j}^k \in \mathbb{C},$$

where, if $k^1 = (k_1,k_2,k_3)$ and $k^2 = (k_4,k_5,k_6)$, we denote $|k| = |k_1| + \cdots + |k_6|$. For further use, we define the norms

$$\begin{aligned} ||f_n|| &= \sum_{|k|=n} \sum_{j\in\mathbb{Z}} |f_{n,j}^k|, \\ ||f_n||_\rho &= \sup_{(u,v)\in B_\rho,\, \theta\in\mathbb{T}^1} |f_n(u,v,\theta)|, \end{aligned}$$

where B_ρ denotes the ball of radius ρ –with respect to the Euclidean metric– centred at the origin.

4.4.2. *Lemmas.* The following lemmas are slight modifications of lemmas contained in [10] (see also [19]), in order to include the periodic time dependence.

Lemma 4.1. *Assume that*

$$\begin{aligned} ||\alpha_6|| \sum_l m_l ||A_{n-1}^l|| &\le S_{n-1}, \\ ||\alpha_6|| \sum_l m_l ||A_n^l|| &\le S_n, \end{aligned}$$

for some $n \ge 2$ and positive constants S_{n-1} and S_n. Then, for $k > n$ one has $||H_k|| \le S_k$, where $\{S_k\}_{k>n}$ is a sequence of positive numbers recursively defined by

$$S_{k+1} = c_1 \left(\frac{2k+1}{k+1} c_2 S_k + \frac{k}{k+1} c_3 S_{k-1} \right), \qquad k \ge n,$$

where

$$\begin{aligned} c_1 &= \max_l c_1^l \quad \textit{where} \quad c_1^l = \left\| \frac{1}{x_l^2(\theta) + y_l^2(\theta)} \right\|, \\ c_2 &= \max_l c_2^l \quad \textit{where} \quad c_2^l = ||x_l(\theta)x + y_l(\theta)y||, \\ c_3 &= ||x^2+y^2+z^2||, \end{aligned}$$

where x, y and z are linear functions of q and p with coefficients that depend periodically on time, and the norms have been taken with respect to the variables p and q.

Proof. For all $n \ge 2$ one has $H_{n+1} = -\alpha_6(\theta) \sum_l m_l A_{n+1}^l$, where

$$A_{n+1}^l = \frac{1}{x_l^2(\theta)+y_l^2(\theta)} \left(\frac{2n+1}{n+1} (x_l(\theta)x + y_l(\theta)y) A_n^l - \frac{n}{n+1} (x^2+y^2+z^2) A_{n-1}^l \right).$$

If we take norms,

$$||A_{n+1}^l|| \le c_1^l \left(\frac{2n+1}{n+1} c_2^l ||A_n^l|| + \frac{n}{n+1} c_3 ||A_{n-1}^l|| \right).$$

Thus,

$$\|H_{n+1}\| \le \|\alpha_6\| \sum_l m_l \|A^l_{n+1}\| \le c_1 \left(\frac{2n+1}{n+1} c_2 S_n + \frac{n}{n+1} c_3 S_{n-1} \right) = S_{n+1}.$$

□

LEMMA 4.2. *Let us suppose that*

$$\begin{aligned} \|\alpha_6\| \sum_l m_l \|A^l_{n-1}\| &\le S_{n-1}, \\ \|\alpha_6\| \sum_l m_l \|A^l_{n}\| &\le S_{n}, \end{aligned}$$

for any $n \ge 2$ and positive constants S_{n-1} and S_n. Then, for $k > n$, one has $\|H_k\| \le h^{k-n+1}E$, with

$$\begin{aligned} E &= S_{n-1}, \\ h &= max \left(\frac{S_n}{S_{n-1}}, c_1 c_2 + \sqrt{c_1^2 c_2^2 + c_1 c_3} \right), \end{aligned}$$

where c_1, c_2 and c_3 are defined in Lemma 4.1.

Proof. We use induction. If $k = n-1$, then $\|H_{n-1}\| \le S_{n-1} = E$. If $k = n$, it follows that $\|H_n\| \le S_n = hE$ and, hence,

$$h \ge \frac{S_n}{S_{n-1}}. \tag{8}$$

For the case $k > n$, we assume that the result is true for k and we will show that it also holds for $k+1$.

$$\begin{aligned} S_{k+1} &= c_1 \left(\frac{2k+1}{k+1} c_2 S_k + \frac{k}{k+1} c_3 S_{k-1} \right) \\ &\le c_1 \left(\frac{2k+1}{k+1} c_2 h^{k-n+1} E + \frac{k}{k+1} c_3 h^{k-n} E \right). \end{aligned}$$

Imposing the right part of the inequality to be smaller than $h^{k-n+2}E$ we obtain

$$\frac{2k+1}{k+1} c_1 c_2 h + \frac{k}{k+1} c_1 c_3 \le h^2. \tag{9}$$

Both inequalities (8) and (9) are satisfied by h. □

5. TRUNCATED NORMAL FORM

Here we will compute a high order normal form for the expansion of the Hamiltonian obtained in the previous section. This initial expansion is already a normal form of degree 2, so here we will directly focus on the explicit computation to higher orders, as well as on obtaining explicit expansions for the change of variables.

5.1. **Normal form of order higher than 2.**

For the computation of the normal form, we use the Lie series method as described in [27] –to avoid using the Lie triangle–, but with the modifications introduced in [24] (see also [30, 49]) to deal with the periodic time-dependence. The purpose of the normalizing transformation is to suppress the maximum number of terms in the Hamiltonian.

Let us start by describing a general step of the normalizing process. Suppose that the Hamiltonian is already in normal form up to degree $r-1$:

$$H = \omega_{sat} p_\theta + H_2(q,p) + \sum_{j=3}^{r-1} H_j(q,p) + H_r(q,p,\theta) + H_{r+1}(q,p,\theta) + \cdots$$

where $H_r(q,p,\theta) = \sum_{|k|=r} h_r^k(\theta) q^{k^1} p^{k^2}$, $h_r^k(\theta) = \sum_j h_{r,j}^k e^{ji\theta}$ and $k = (k^1, k^2) \in \mathbb{Z}^3 \times \mathbb{Z}^3$ is a multi-index.

We want to make a change of variables that removes the θ-dependence in H_r and suppress the maximum number of monomials of H_r. Let us call G_r the generating function of the canonical transformation we are looking for,

$$G_r = G_r(q,p,\theta) = \sum_{|k|=r} g_r^k(\theta) q^{k^1} p^{k^2}, \qquad g_r^k(\theta) = \sum_j g_{r,j}^k e^{ji\theta}. \tag{10}$$

If we apply the transformation defined by the time 1 flow of the Hamiltonian G_r (for more details, see the Appendix A of [27]), we easily see that the terms of degree r of the transformed Hamiltonian, H_r', are given by

$$H_r' = H_r + \{\omega_{sat} p_\theta, G_r\} + \{H_2, G_r\} \equiv H_r + \omega_{sat} \frac{\partial G_r}{\partial \theta} + \{H_2, G_r\}.$$

We select the Fourier coefficients $g_{r,j}$ of (10) such that H_r' has the simplest possible form:

$$g_r^k(\theta) = \begin{cases} \dfrac{i h_{r,0}^k}{\langle \omega, k^2 - k^1 \rangle} + \displaystyle\sum_{j \neq 0} \frac{h_{r,j}^k}{ij\omega_{sat} - i \langle \omega, k^2 - k^1 \rangle} e^{ji\theta} & \text{if} \quad k^1 \neq k^2, \\ \displaystyle\sum_{j \neq 0} \frac{h_{r,j}^k}{ij\omega_{sat}} e^{ji\theta} & \text{if} \quad k^1 = k^2, \end{cases}$$

Of course, we are assuming that the frequencies $\omega = (\omega_1, \omega_2, \omega_3)$ and ω_{sat} satisfy a non-resonance condition, $ij\omega_{sat} - i\langle \omega, k \rangle \neq 0$, $j \in \mathbb{Z}$, $k \in \mathbb{Z}^3$. In fact, as we will only apply this process up to a finite order in the variables (q,p), and the Fourier series are truncated to a finite order, this condition is only needed up to suitable values of $|j|$ and k. In fact, it is automatically checked before computing the function G_r, for each r. In our case, this non-resonance condition is satisfied up to the orders we have worked with.

The H_r' obtained with such a G_r does not depend on time, and it only depends on monomials of the form $q^{k^1} p^{k^2}$, with $k^1 = k^2$. The new Hamiltonian obtained with this change of variables is

$$H' = H + \{H, G_r\} + \frac{1}{2!} \{\{H, G_r\}, G_r\} + \cdots,$$

and satisfies that

$$H' = \omega_{sat} p_\theta + H_2(q,p) + \sum_{j=3}^{r-1} H_j(q,p) + H_r'(q,p) + H_{r+1}'(q,p,\theta) + \cdots,$$

is in normal form up to degree r. Hence, we can rename the Hamiltonian as H, and repeat the same process as before and compute the normal form for the terms of degree $r+1$.

1	0	0	-8.0473403414658348e-02	0.0000000000000000e+00
0	1	0	9.9668687782955701e-01	0.0000000000000000e+00
0	0	1	1.0000674413904136e+00	0.0000000000000000e+00
2	0	0	5.6007414394589805e-01	-1.8705256953566430e-13
1	1	0	-1.5540007094294600e-01	-9.3830451518209680e-15
0	2	0	5.5094910495712413e-03	1.0717280513316625e-16
1	0	1	5.4161643846023226e-02	-6.2140551599726659e-15
0	1	1	6.6064951514490360e-03	1.2257344054847067e-16
0	0	2	-3.4086514191576233e-04	9.5191394827757230e-22
3	0	0	1.7076591917555746e+01	-7.8087823960270605e-09
2	1	0	2.5312327640336463e+00	5.9890652038702482e-09
1	2	0	1.2040133893299085e+00	7.5183303416244784e-10
0	3	0	-1.7301900678281523e-03	4.4060011855097767e-12
2	0	1	-2.0884087969793064e-01	-3.6110568734989503e-10
1	1	1	1.3097674563771786e+00	1.6810633045057165e-10
0	2	1	-8.8065932627078847e-03	1.8072038419138380e-12
1	0	2	-3.8394202697275989e-02	-6.8093926120365380e-12
0	1	2	-8.1760590356997620e-03	-1.9530188730672947e-13
0	0	3	4.8057053869314466e-04	-3.8350420390170530e-14

TABLE 2. Coefficients of the normal form, up to degree 3 in the actions. The first three columns contain the exponents of the actions, and the fourth and fifth columns are the real and imaginary part of the coefficients. Imaginary parts must be zero, but they are not due to the roundoff errors of the floating point arithmetic.

After performing all this changes up to a suitable degree $n = N$, the Hamiltonian takes the form

$$H = \mathcal{N}(q_1p_1, q_2p_2, q_3p_3) + \mathcal{R}(q_1, q_2, q_3, p_1, p_2, p_3, \theta), \tag{11}$$

where $\mathcal{N}$ denotes the normal form (that only depends on the products q_jp_j) and $\mathcal{R}$ is the remainder. Finally, we will write the normal form $\mathcal{N}$ again in real action-angle coordinates. This can be easily achieved by using the (canonical) transformation,

$$q_j = I_j^{1/2}\exp(i\varphi_j), \quad p_j = -iI_j^{1/2}\exp(-i\varphi_j), \quad j = 1, 2, 3. \tag{12}$$

It is not difficult to see that $\mathcal{N}$, in these coordinates, does not depend on the angles φ_j but only on the actions I_j,

$$\mathcal{N} = \sum_{|k|=1}^{[N/2]} h_k I_1^{k_1} I_2^{k_2} I_3^{k_3}, \qquad k \in \mathbb{Z}^3, \quad h_k \in \mathbb{R}.$$

Values for the coefficients h_k can be found in Table 2.

Later, we will also use this normalized Hamiltonian in the real coordinates (x, y), defined as

$$I_j = \frac{1}{2}(x_j^2 + y_j^2), \qquad j = 1, 2, 3.$$

These coordinates can also be defined from the coordinates (q, p) of (11) by

$$q_j = \frac{x_j - iy_j}{\sqrt{2}}, \quad p_j = \frac{-ix_j + y_j}{\sqrt{2}}, \quad j = 1, 2, 3. \tag{13}$$

Note that this is the inverse of (5).

5.2. **Changes of variables.** With a similar process based on the use of Lie series, we have also computed explicit expressions for the transformation from the initial variables of (6) to the final variables (see [24, 27] for more details). This change of variables is also a truncated power series up to degree N, that will be used in the forthcoming sections to send information from the normal form coordinates to the initial ones.

5.3. **Invariant tori.** In the previous sections we have obtained a change of variables that brings the initial Hamiltonian (2) into the form $H = \mathcal{N} + \mathcal{R}$, where $\mathcal{N}$ is an autonomous, integrable Hamiltonian system, and $\mathcal{R}$ is a remainder of order 17 with respect to the distance to the periodic orbit. Hence, we can neglect the term $\mathcal{R}$ and take $\mathcal{N}$ as a good approximation for the dynamics, at least near the periodic orbit.

The dynamics of the integrable normal form $\mathcal{N}$ is very simple: as $\mathcal{N}$ only depends on the action coordinates, the equations of motion are

$$\dot{I} = -\nabla_{\varphi}\mathcal{N}(I) \equiv 0, \qquad \dot{\varphi} = \nabla_I \mathcal{N}(I) \equiv \Omega(I), \quad I \in \mathbb{R}^3, \quad \varphi \in \mathbb{T}^3. \tag{14}$$

These equation can be easily integrated:

$$I = I_0, \qquad \varphi = \Omega(I_0)t + \varphi_0, \tag{15}$$

Therefore, the phase space is completely foliated by a 3-parametric family of invariant tori (I_0 is the parameter) and, on each torus $I = I_0$, there is a linear flow with frequency $\Omega(I_0)$. If the frequencies (i.e., the components of the vector $\Omega(I_0)$) are linearly independent over the rationals then the torus $I = I_0$ is filled densely by any trajectory starting on it. If the frequencies are linearly dependent over the rationals, then the orbits on this torus are not dense: if there are ℓ_i independent frequencies, the torus $I = I_0$ contains a $(3-\ell_i)$-parametric family of ℓ_i dimensional tori, being each one densely filled by any trajectory starting on it. These tori of dimension ℓ_i are known as lower dimensional tori, while the tori of dimension 3 are called maximal dimensional ones.

The effect of the remainder $\mathcal{R}$ on these tori is studied by the KAM theory. Essentially, the KAM theorem ensures that the tori whose frequencies satisfy a suitable Diophantine condition of the kind,

$$\langle k, \Omega(I_0)\rangle \geq \frac{c}{|k|^{\tau}},$$

are not destroyed by the perturbation, but only slightly deformed. Under generic conditions, it can be proved that the measure of the tori not preserved by the effect of the remainder is bounded by an exponentially small quantity with respect to the periodic orbit ([33, 32, 35]). This implies that, from a practical point of view, the phase space of the complete system $\mathcal{N} + \mathcal{R}$ seems, near the origin, foliated by invariant tori, since the measure of the set of non quasi-periodic motions is too small to be seen with the standard floating point arithmetic of the computer.

Let us now consider the frequency map of the normal form,

$$\Omega : B \subset \mathbb{R}^3 \to \mathbb{R}^3,$$

where $\Omega \equiv \nabla_I \mathcal{N}$, and B is an open neighbourhood of the origin such that the remainder $\mathcal{R}$ is sufficiently small or, in other words, such that the normal form provides a sufficiently good approximation to the dynamics (later, in Section 5.4, we will discuss how to estimate such a domain). The vector $\Omega(0)$ is the vector of normal frequencies of the periodic orbit (the values $(\omega_1,\omega_2,\omega_3)$ obtained in Section 4.2). Consider the line $I_\lambda=(\lambda,0,0)$, $|\lambda|\le\lambda_0$, and the values $\Omega(I_\lambda)$. For any value of λ, the corresponding trajectory in (14) is sent by (12) into a periodic orbit in the (q,p) coordinates; the frequency of this orbit is $\Omega_1(I_\lambda)$, and the normal frequencies are $\Omega_2(I_\lambda)$ and $\Omega_3(I_\lambda)$. Similar families can be obtained using $I_\lambda=(0,\lambda,0)$ and $I_\lambda=(0,0,\lambda)$. These families of periodic orbits can be seen as the Lyapunov families (of periodic orbits) around the origin of the normal form. When these families are sent (through the changes we have computed before) to the coordinates of the BCCP Hamiltonian (2), they "gain" the frequency of the periodic orbit and become quasi-periodic orbits –with two basic frequencies– near the periodic orbit replacing L_5. Of course, this does not prove the existence of these families of quasi-periodic solutions around the periodic orbit because, during the computations, we have neglected the remainders. The proof of persistence requires a KAM theorem adapted to the lower-dimensional case, see [33].

We can also consider two-parametric families $I_{\lambda_1,\lambda_2}=(\lambda_1,\lambda_2,0)$. This will produce a two-parametric family of two-dimensional tori on the normal form, with frequencies $\Omega_1(I_{\lambda_1,\lambda_2})$ and $\Omega_2(I_{\lambda_1,\lambda_2})$, and normal frequency $\Omega_3(I_{\lambda_1,\lambda_2})$. This family gives rise, in the initial BCCP coordinates, to a two-parametric family of quasi-periodic orbits with three basic frequencies. Finally, we can use three non-zero parameters $\lambda_{1,2,3}$ to obtain three dimensional tori in the normal form, that correspond to four dimensional tori for the BCCP problem. Therefore, the normal form gives a complete description of the kind of quasi-periodic orbits we can find near the periodic orbit replacing L_5.

Finally, we will use this normal form to compute some quasi-periodic motions near the periodic orbit. The process will be as follows. First, we will select a value $I_0\in\mathbb{R}^3$ –later we will discuss this selection with more detail– and we will compute the vector $\Omega(I_0)=\nabla_I\mathcal{N}(I_0)$ (we recall that $\mathcal{N}$ is a polynomial in I). Given a phase φ_0 (for these examples, we have simply taken $\varphi_0=0$), it is then not difficult to use (15) to tabulate points of the corresponding trajectory on the torus $I=I_0$. Finally, using the changes of variables, we can send these points to the initial (synodical) coordinates of the BCCP model.

Figures 10, 11 and 12 are examples of these computations. More concretely, Figure 10 displays two different projections of a two dimensional torus of the vertical family –the family that "grows" in the (z,p_z) direction–. Figure 11 are projections of two different two dimensional tori contained in the $z=p_z=0$ plane. Finally, Figure 12 displays the projections of a three and a fourth dimensional torus. All these graphics have been obtained computing 10,000 points, with a time step of 0.1 units. See the captions for more details.

We also note that, in this way, it is possible to compute quasi-periodic orbits with prescribed set of frequencies Ω_0, provided that Ω_0 belongs to the domain B where the normal form is accurate.

5.4. **A lower bound on the diffusion time.** As it has been explained in the previous section, the dynamics described by the normal form is quasi-periodic. This means that, for the normal form, the origin is Lyapunov stable. Of course, this picture can be changed by the effect of the remainder $\mathcal{R}$. For this reason, in this section we will focus on the determination of a region B in the actions space, such that any trajectory starting inside B remains near B for a time of the order

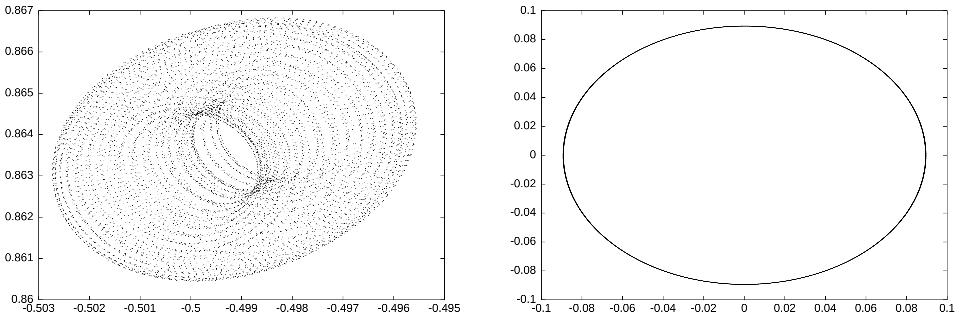

FIGURE 10. Projection on the (x, y) (left) and on the (z, p_z) (right) planes of an elliptic two-dimensional invariant torus of the vertical family near the periodic orbit that replaces L_5. The intrinsic frequencies are ω_{sat} and $\omega_3 = 1.000064737$. The normal ones are $\omega_1 = -0.08025736934$ and $\omega_2 = 0.9967131749$.

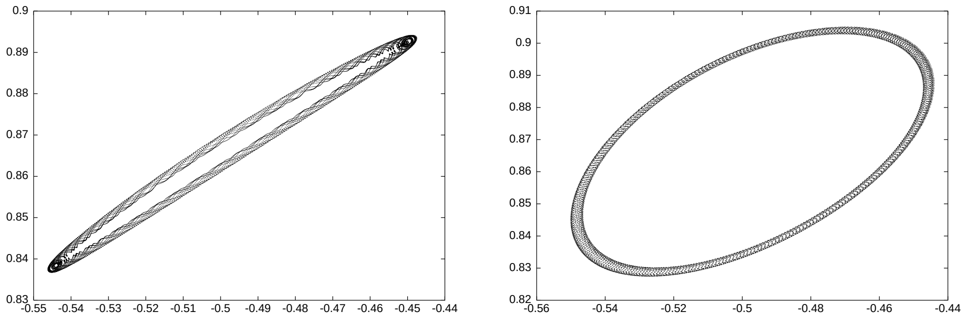

FIGURE 11. Projections on the (x, y) plane of two tori, belonging to the two planar two-dimensional invariant tori families near the periodic orbit that replaces L_5. The intrinsic frequencies of the left figure one are ω_{sat}, $\omega_1 = -0.08042851476$ and the normal ones are $\omega_2 = 0.9966806656$, $\omega_3 = 1.000069607$. For the right figure one the intrinsic frequencies are ω_{sat}, $\omega_2 = 0.9966912842$ and the normal ones $\omega_1 = -0.08053537024$, $\omega_3 = 1.000070082$.

of the age of the Solar system. The method to compute such a region is based on bounding the remainder $\mathcal{R}$, and it is based on the procedures used in [19], [48] and [30].

5.4.1. *Norms.* We will use the norms defined in Section 4.4.1. Here, the sup norm $||.||_\rho$ will be always taken for real values of the variables. If $f_n(x, y, \theta)$ and $g_m(x, y, \theta)$ denote homogeneous polynomial of degrees n and m, we have that

$$\begin{aligned} ||\{f_{n_1}, g_{n_2}\}|| &\leq n_1 n_2 ||f_{n_1}|| ||g_{n_2}||, \\ ||f_n||_\rho &\leq \rho^n ||f_n||. \end{aligned}$$

The proof is a straightforward generalisation of the autonomous case ([18]).

5.4.2. *Bounding the effect of the remainder.* Let us consider a trajectory $(x(t), y(t))$ for the Hamiltonian (11) in the coordinates (x, y) defined by (13). We define the

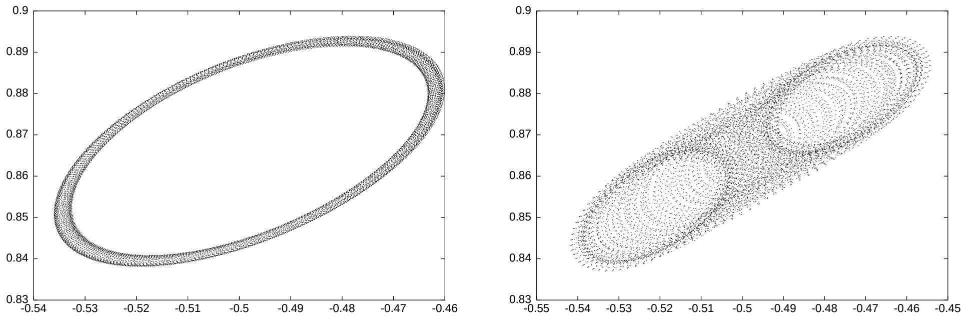

FIGURE 12. Left: Projection on the (x, y) plane of an elliptic three-dimensional invariant torus of the vertical family near the periodic orbit that replaces L_5. The intrinsic frequencies are ω_{sat}, $\omega_2 = 0.9966904013$ and $\omega_3 = 1.000068625$. The normal one is $\omega_1 = -0.08049355163$. Right: Projection on the (x, y) plane of an elliptic fourth-dimensional invariant torus of the vertical family near the periodic orbit that replaces L_5. The frequencies are ω_{sat}, $\omega_1 = -0.08045369737$, $\omega_2 = 0.9966878607$ and $\omega_3 = 1.000068109$.

quantity $\rho(t)$ as the distance of the trajectory to the origin,

$$\rho(t)^2 = \sum_{j=1}^{3} (x_j(t)^2 + y_j(t)^2).$$

As $I_j(t) = \frac{1}{2}(x_j(t)^2 + y_j(t)^2)$, $j = 1, 2, 3$, we have that

$$\frac{1}{2}\rho(t)^2 = \sum_{j=1}^{3} I_j(t).$$

Then,

$$\rho\dot{\rho} = \sum_{j=1}^{3} \dot{I}_j = \sum_{j=1}^{3} \{I_j, H\} = \sum_{j=1}^{3} \{I_j, \mathcal{R}\}, \tag{16}$$

where we have used that $H = \mathcal{N} + \mathcal{R}$, and that $\mathcal{N}$ only depends on the actions I_j. To continue with this process, we will make use of the following estimation.

LEMMA 5.1. *Let $f_n(x, y, \theta)$ be an homogeneous polynomial of degree n in (x, y) coordinates with time dependent coefficients and $I_j = \frac{1}{2}(x_j^2 + y_j^2)$ with $j = 1, 2, 3$. Then,*

$$\left\| \left\{ \sum_{j=1}^{3} I_j, f_n \right\} \right\| \le n \|f_n\|.$$

Proof. It is based on Lemma A.3 in [18]. As we have

$$\left\{ \sum_{j=1}^{3} I_j, f_n \right\} = \sum_{|k^1|+|k^2|=n} \left(\sum_{j=1}^{3} (k_j^2 \frac{x_j}{y_j} - k_j^1 \frac{y_j}{x_j}) \right) \left(\sum_l f_{n,l}^k(\theta) \right) x^{k^1} y^{k^2},$$

taking bounds, we obtain

$$
\begin{aligned}
\left\| \left\{ \sum_{j=1}^{3} I_j, f_n \right\} \right\| &\leq \sum_{|k^1|+|k^2|=n} \left(\sum_{j=1}^{3} (k_j^1 + k_j^2) \right) \left(\sum_{l} |f_{n,l}^{k}(\theta)| \right) \\
&= n \sum_{|k^1|+|k^2|=n} \sum_{l} |f_{n,l}^{k}(\theta)|.
\end{aligned}
$$

□

Now we can continue from formula (16). If we write $\mathcal{R} = \sum_{k>N} \mathcal{R}_k$ ($\mathcal{R}_k$ denotes an homogeneous polynomial of degree k), we can take absolute values in both sides of (16) and, using the bound in Lemma 5.1 we have that (16) becomes

$$|\dot{\rho}| \leq \sum_{k>N} k \|\mathcal{R}_k\| \rho^{k-1}.$$

Now we define the function

$$z(\rho) = \sum_{k>N} k \|\mathcal{R}_k\| \rho^{k-1},$$

and, therefore, to estimate the diffusion speed (given by $\dot{\rho}$) we need to produce bounds on this function. Of course, the main problem is that, in the normal form process, we have not obtained the terms $\mathcal{R}_k$ for $k > N$. As we cannot compute those terms for all $k > N$, we will try to derive bounds on them. So, we start by computing the norms of the initial expanded Hamiltonian up to degree N and, with the recurrence given in Lemma 4.1, we compute explicit bounds on the terms of the Hamiltonian up to a given degree $\widehat{N}$. Then, we transform (numerically) these norms using the sequence of changes given by the generating functions used to put the Hamiltonian in normal form up to degree N. For example, in step r ($r = 3, \ldots, N$) we have the exact norms of the terms 2 to N of the Hamiltonian in normal form up to degree $r-1$ and a bound on the norms of the terms $N+1$ to $\widehat{N}$ of the same Hamiltonian. To obtain bounds of the norms of the Hamiltonian in normal form up to degree r, we use the same process as described in Section 5.1, but only using norms in the formulas:

$$
\begin{aligned}
\|\bar{H}_k\| &\leq \|H_k\| + \| \{H_{k-r+2}, G_r\} \| + \frac{1}{2!} \| \left\{ \{H_{k-2(r-2)}, G_r\}, G_r \right\} \| + \cdots \\
&\leq \|H_k\| + (k-r+2) r \|H_{k-r+2}\| \|G_r\| \\
&\quad + \frac{1}{2!} (k - 2(r-2))(k-r+2) r^2 \|H_{k-2(r-2)}\| \|G_r\|^2 + \cdots ,
\end{aligned}
$$

for $N < k \leq \widehat{N}$. After the last step ($r = N$), we have obtained an array of bounds of the norms of the terms from degree $N+1$ to $\widehat{N}$ of the Hamiltonian in normal form up to degree N. These are the bounds we were looking for.

Then, we can approximate the function $z(\rho)$:

$$z(\rho) \approx \sum_{k=N+1}^{\widehat{N}} k \|\mathcal{R}_k\| \rho^{k-1}.$$

Note that, if $\widehat{N}$ is sufficiently large, the effect of the remainder $\sum_{k>\widehat{N}} k \|\mathcal{R}_k\| \rho^{k-1}$ can be neglected. For the final calculations, in this paper we have used the values $N = 16$ and $\widehat{N} = 99$.

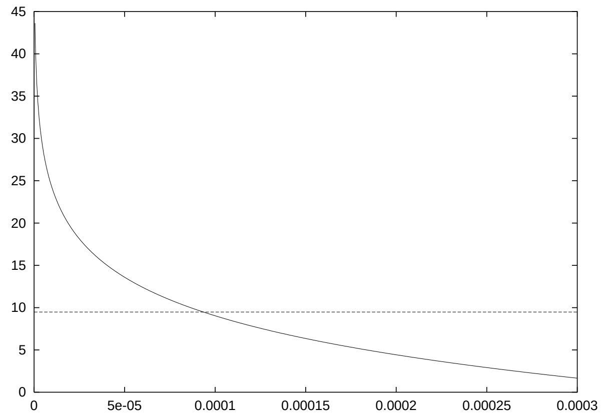

FIGURE 13. Plot of the function $\log(T_{\rho_0})$ and the estimated age of the Solar System $\log(T_S) = 9.4771213$ is marked with an horizontal line.

5.4.3. *Region of effective stability.* Assume that we select an initial condition inside a ball B_{ρ_0} and that we want the orbit to remain inside B_ρ ($\rho > \rho_0$) during a time span of length T. Then, the values ρ_0, ρ and T satisfy

$$T = \int_{\rho_0}^{\rho} \frac{du}{z(u)}. \tag{17}$$

So, if we write $\rho = \sigma\rho_0$ and we select a value $\sigma > 1$, equation (17) defines a function $T = T(\rho_0)$. This function can be tabulated numerically, and it is plotted in Figure 13. In this paper, we have used the value $\sigma = 2.1861$. This value of σ is chosen to compare these results with the ones obtained using a first integral. See Section 6.3.2 for more details.

Then, if we choose $T = T_S \equiv 3 \times 10^9$ as an estimation of the age of the Solar system (we recall that 2π is the period of the orbit of Jupiter), we can easily find the initial radius ρ_0 for which any orbit starting in the ball B_{ρ_0} lies inside the ball $B_{\sigma\rho_0}$ for this time span T_S. The result obtained here is $\rho_0 = 9.3539 \times 10^{-5}$.

5.4.4. *Going back to synodical coordinates.* The last step is to send this ball to the initial coordinates of the BCCP. We first note that, due to the time dependence, the resulting stability region moves around the periodic orbit substituting L_5. Here, in order to compare the results obtained with the normal form, first integrals and direct numerical simulation, we will use the following scheme:

a) Compute a 2-D mesh of points, in the synodical BCCP coordinates x and y, around the position of the periodic orbit for $t = 0$.
b) Each point (x, y) of this mesh is completed to a 6-D point by adding the z, p_x, p_y and p_z coordinates of the periodic orbit for $t = 0$.
c) These points are sent to the real normal form coordinates, so we can test whether the point is inside the ball B_{ρ_0} or not.
d) The initial (x, y) coordinates of the points that are mapped into B_{ρ_0} are plotted.

The result of this procedure is shown in Figure 14 where each point of d) has been marked with a black dot. More comments in Section 7.

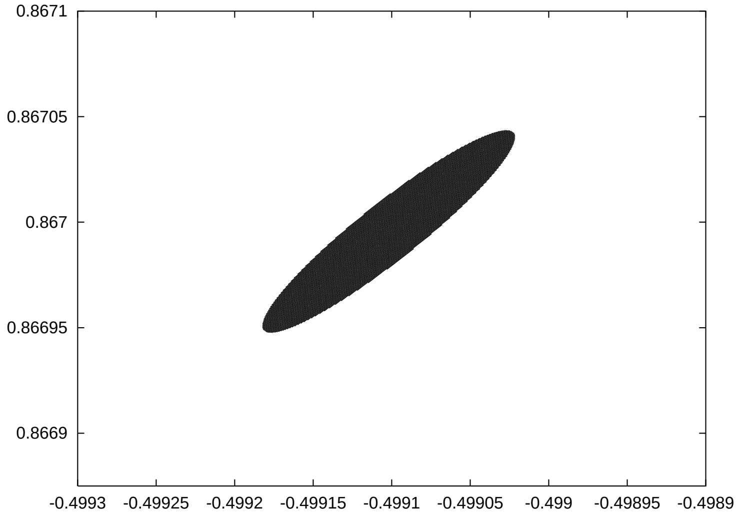

FIGURE 14. Region of effective stability from the normal form computation. The region has been computed around the position for $t = 0$ of the periodic orbit replacing L_5. The axis are the x and y synodical coordinates of the BCCP used in (2) and in Figure 8.

6. Approximate first integrals

This section is devoted to the computation of an approximate first integral for the BCCP Hamiltonian (2). Then, we will use this approximate first integral for computing a region of effective stability around the periodic orbit replacing L_5. This process is based on the methods used in [18, 10], with the necessary modifications to include the periodic time-dependence of the Hamiltonian. This is an alternative procedure to the normal form computations for estimating regions of effective stability.

6.1. **Numerical computation.** We start with the Hamiltonian expanded in complex coordinates, as it has been explained in Section 4,

$$H(q,p,\theta,p_\theta) = \omega_{sat} p_\theta + H_2(q,p) + \sum_{n\geq 3} H_n(q,p,\theta),$$

where H_2 is in the diagonal form (6), and H_n are homogeneous polynomials of degree n. As before, we have introduced p_θ as the conjugate variable of θ, so the Hamiltonian is now autonomous. We look for an approximate first integral as a truncated Taylor-Fourier expansion,

$$F(q,p,\theta) = \sum_{n=2}^{N} F_n(q,p,\theta),$$

where, as usual, F_n stands for an homogeneous polynomial of degree n in the variables (q,p), with coefficients that are (truncated) Fourier series in the angle θ. Note that F does not depend on p_θ; the reasons for this selection will be clear later on.

It is known that, if F is a first integral for the flow of the Hamiltonian H, then $\{H, F\} = 0$ (for a summary of basic properties of Hamiltonian systems, see Appendix A of [27]). This equation gives a recursive way of computing the coefficients of the expansion of F: taking into account the form of H, we have

$$\{\omega_{sat} p_\theta, F\} + \{H_2, F\} = -\left\{\sum_{n\geq 3} H_n, F\right\}. \tag{18}$$

Now we use the expansion for F, and we select

$$F_2 = i\sum_{j=1}^{3} q_j p_j. \tag{19}$$

As $\{H_2, F_2\} = 0$, equation (18) reads "0=0" for $n = 2$. So, we will focus on the case $n > 2$. Assume now that we know the values F_m for $2 \leq m < n$, and we want to compute F_n. From (18), we have

$$\sum_{n=3}^{N} -\omega_{sat}\frac{\partial F_n}{\partial \theta} + \sum_{n=3}^{N}\{H_2, F_n\} = -\sum_{n\geq 3}\sum_{j=3}^{n}\{H_j, F_{n-j+2}\}$$

In this equation, we select all the terms of degree n to obtain

$$-i\omega_{sat}\sum_{|k|=n}\left(\sum_j j f_{n,j}^k e^{ij\theta}\right) q^{k^1} p^{k^2} + \{H_2(q,p), F_n(q,p,\theta)\} = C_n(q,p,\theta), \tag{20}$$

where $f_{n,j}^k$ is the j-Fourier coefficient of $f_n^k(\theta)$, $F_n(q,p,\theta) = \sum_{|k|=n} f_n^k(\theta) q^{k^1} p^{k^2}$ and

$$C_n(q,p,\theta) = -\sum_{j=3}^{n}\{H_j(q,p,\theta), F_{n-j+2}(q,p,\theta)\}$$

Note that C_n only depends on values of F_m that are known. Hence, we can write it as

$$C_n(q,p,\theta) = \sum_{|k|=n}\left(\sum_j c_{n,j}^k e^{ij\theta}\right) q^{k^1} p^{k^2},$$

where the coefficients $c_{n,j}^k$ are known. Then, equation (20) can be easily solved to find F_n:

$$f_{n,j}^k = \frac{i c_{n,j}^k}{j\omega_{sat} - \langle k^2 - k^1, \omega\rangle}. \tag{21}$$

Hence, we have derived a recurrent procedure to generate the formal expansion of the first integral. This process is very similar to the one used in [10], but with the necessary modifications to take into account the periodic time dependence.

The reason for selecting F_2 as (19) is that, in real coordinates, it corresponds to a positive definite quadratic form,

$$F_2 = \sum_{j=1}^{3}\frac{1}{2}(x_j^2 + y_j^2). \tag{22}$$

We will show that, using this positive definite character of F_2 on a suitable domain, F has a bounded drift for a time of $T_S = 3 \times 10^9$ and that, on the same domain, the level surfaces of F still act as a barrier to the diffusion. Note that, in [10], the authors use three independent first integrals, corresponding to the selection

$$F_2^{(j)} = \frac{1}{2}(x_j^2 + y_j^2), \qquad j = 1, 2, 3,$$

and they bound the drift of these three integrals. Hence, each integral is used to bound the diffusion in the corresponding direction (x_j, y_j). Here, we use a single integral, that is a positive definite combination of these three. In this way, we only need to compute and control a single first integral. Finally, note that the integral does not contain the variable p_θ, so we do not obtain bounds on the diffusion of this variable. We note that p_θ has been introduced to autonomize the Hamiltonian, and has no physical meaning, so there is no need in bounding the drift of such variable. In fact, the diffusion in this variable can be seen as a diffusion respect to the initial phase taken for the angular variable θ, which is irrelevant for our purposes.

As a side comment, we want to note that the formal existence of these integrals to all orders is not a trivial question. Looking at (21) it is clear that the following two conditions are required:

a) ω_{sat} and ω must satisfy that

$$j\omega_{sat} - \langle k, \omega\rangle \neq 0, \quad \forall\, j \in \mathbb{Z}, \quad \forall\, k \in \mathbb{Z}^3 \text{ such that } |j| + |k| \neq 0,$$

b) if $j = 0$ and $k^1 = k^2$, the value $c_{n,j}^k$ must vanish.

If ω_{sat} and ω are known, condition a) can be in principle verified. Condition b) is, however, much more involved. See [10] for a discussion.

6.2. **Bounding the diffusion.** We will start using the expansion of the Hamiltonian in complex coordinates obtained in 4. Thus, the Hamiltonian looks like:

$$H = \omega_{sat} p_\theta + \sum_{j=1}^{3} i\omega_j q_j p_j + \sum_{n\geq 3} H_n(q, p, \theta).$$

We will assume that we have computed a truncation F (to degree N) of a formal first integral. Then, both this Hamiltonian and F can be put again into real form using (13). Hence, they will have the form

$$\begin{aligned} H &= \omega_{sat} p_\theta + \sum_{j=1}^{3} \frac{\omega_j}{2}\left(x_j^2 + y_j^2\right) + \sum_{n\geq 3} H_n(x, y, \theta), \\ F &= \sum_{j=1}^{3} \frac{1}{2}\left(x_j^2 + y_j^2\right) + \sum_{n=3}^{N} F_n(x, y, \theta). \end{aligned}$$

Note that the variation of the values of F on a given trajectory of the Hamiltonian is not constant –F is not an exact first integral–, and that this variation can be written as

$$\dot F = \left\{F(q, p, \theta), H(q, p, \theta, p_\theta)\right\}.$$

From the equations in Section 6.1, it is easy to see that

$$\dot F = \sum_{n>N} \sum_{l=3}^{N} \left\{F_l, H_{n-l+2}\right\} + \sum_{n>N} \left\{F_2, H_n\right\}. \tag{23}$$

We will follow the same scheme as in [10]. So, we will use Lemmas in Section 4.4.2 to estimate the size of the terms in the Hamiltonian that have not been numerically computed. The idea is the following: we have computed F (and the expansion of H) up to degree $N=16$. Then, we will select a second degree $\widehat{N}$ (we have used $\widehat{N}=99$) and we will use Lemma 4.1 to bound the norms of the expansion of the Hamiltonian from $n=N+1$ to $n=\widehat{N}$. Finally, the terms of the Hamiltonian of degree $n>\widehat{N}$ will be bounded by means of Lemma 4.2. There are no reasons for the particular selection of $\widehat{N}=99$; we could have chosen an even larger value, but the results do not change in a significant way. The results of applying this procedure to (23) are summarized in the following lemma.

LEMMA 6.1. *Let N and $\widehat{N}$ be integers such that $3 \le N \le \widehat{N}$ and*

$$\begin{array}{lcll} \|H_k\| & \le & S_k & 3 \le k \le \widehat{N}, \\ \|H_k\| & \le & h^{k-\widehat{N}+1}E & k > \widehat{N}, \\ \|F_k\| & \le & Q_k & 3 \le k \le N. \end{array}$$

Then, if $h\rho < 1$,

$$\|\dot{F}\|_\rho \le \mathcal{R}(\rho),$$

where

$$\begin{aligned} \mathcal{R}(\rho) &= \sum_{j=1}^{N-2}(j+2)\rho^j Q_{j+2} \sum_{N-j<l\le\widehat{N}} l\rho^l S_l \\ &\quad + \sum_{j=1}^{N-2}(j+2)\rho^j Q_{j+2}\frac{E}{h^{\widehat{N}}}h\frac{(\widehat{N}+1)(h\rho)^{\widehat{N}+1}-\widehat{N}(h\rho)^{\widehat{N}+2}}{(1-h\rho)^2} + \\ &\quad + \sum_{N<l\le\widehat{N}} l\rho^l S_l + \frac{E}{h^{\widehat{N}}}h\frac{(\widehat{N}+1)(h\rho)^{\widehat{N}+1}-\widehat{N}(h\rho)^{\widehat{N}+2}}{(1-h\rho)^2}. \end{aligned}$$

Proof. See [10]. □

6.3. **A lower bound on the diffusion time.** Assume now that we have an initial condition $(x(0),y(0))$ inside the ball B_{ρ_0}. We are interested in values $\rho>\rho_0$ such that the orbit $(x(t),y(t))$ is contained in B_ρ for all $t\in[0,T_S]$. A sufficient condition to achieve this is that

$$|F_2(x(t),y(t))-F_2(x(0),y(0))| \le \frac{1}{2}(\rho^2-\rho_0^2), \quad 0\le t\le T_S, \tag{24}$$

where F_2 is given by (22). Let us now define

$$\Delta_N(\rho_0,\rho)=\frac{1}{2}(\rho^2-\rho_0^2)-\sum_{j=3}^{N}\|F_j\|(\rho^j+\rho_0^j).$$

It is easy to see that, if $\Delta_N(\rho_0,\rho)\ge 0$ and

$$|F(x(t),y(t))-F(x(0),y(0))|\le\Delta_N(\rho_0,\rho),$$

then, (24) holds. The function $\Delta_N(\rho_0,\rho)$ is used to bound the maximum variation of $F(x,y,\theta)$ on the interval of time $[0,T_S]$ because (24) is a sufficient condition for the trajectory to be inside the ball B_ρ. Note that, due to the particular form of Δ_N, the values ρ_0 and ρ have to be selected sufficiently small to achieve $\Delta_N(\rho_0,\rho)\ge 0$ but, on the other hand, we want Δ_N to be as large as possible, to allow a large

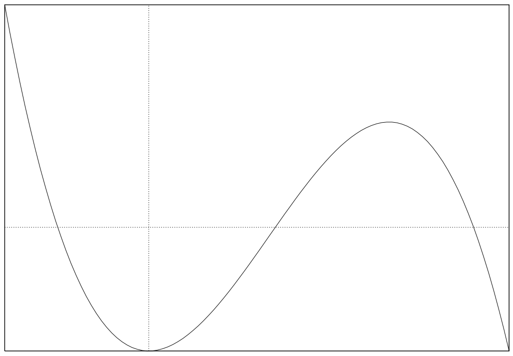

FIGURE 15. Heuristic plot of $\Delta_N(\rho_0, \rho)$ versus ρ for a fixed ρ_0

variation of F with a controlled variation of ρ. Hence, we will carefully select the values ρ_0 and ρ to obtain the largest region of effective stability for time T_S.

So, if $\Delta_N(\rho_0, \rho) \geq 0$ (later we will study this condition in detail), we can bound the escape time as a function of the initial radius,

$$T(\rho_0) = \sup_{\rho} \frac{\Delta_N(\rho_0, \rho)}{\mathcal{R}(\rho)}. \tag{25}$$

6.3.1. *Study of the condition* $\Delta_N(\rho_0, \rho) \geq 0$. As we are interested in values ρ_0 for which $T(\rho_0)$ is large (and positive), we will only focus on the study of values ρ and ρ_0 such that

$$\Delta_N(\rho_0, \rho) = \frac{1}{2}(\rho^2 - \rho_0^2) - \sum_{j=3}^{N} ||F_j||(\rho^j + \rho_0^j) \geq 0.$$

If we fix ρ_0 and study Δ_N as a function of ρ, we observe that there is always a local minimum at $\rho = 0$, and a local maximum at $\rho = \hat{\rho}$ such that

$$\sum_{j=3}^{N} j||F_j||\hat{\rho}^{j-2} = 1.$$

If we increase the value of ρ_0, there is only a change in the values of Δ_N at the local extrema, but not in the points they are achieved. There is just a closed interval, in the positive part of the ρ axis, where the condition holds true (see Figure 15).

Increasing ρ_0, this interval shrinks to one point $\hat{\rho}$. After that, for $\rho_0 > \rho_0^{crit}$ where ρ_0^{crit} is such that $\Delta_N(\rho_0^{crit}, \hat{\rho}) = 0$, the condition is false.

6.3.2. *Final results.* In order to find the supremum in equation (25), we fix ρ_0 and we look for a zero of the equation

$$\frac{\partial \Delta_N}{\partial \rho}(\rho_0, \rho)\mathcal{R}(\rho) - \Delta_N(\rho_0, \rho)\mathcal{R}'(\rho) = 0.$$

We use a Newton method with $\rho = \hat{\rho}$ as initial guess, and this allows to find the supremum in (25). Thus, we solve equation (25) for different ρ_0's and plot T versus ρ_0, see Figure 16.

Afterwards, using inverse interpolation we find the initial radius ρ_0 for which an orbit does not leave the ball B_ρ in a time span of length $T_S = 3 \times 10^9$. The

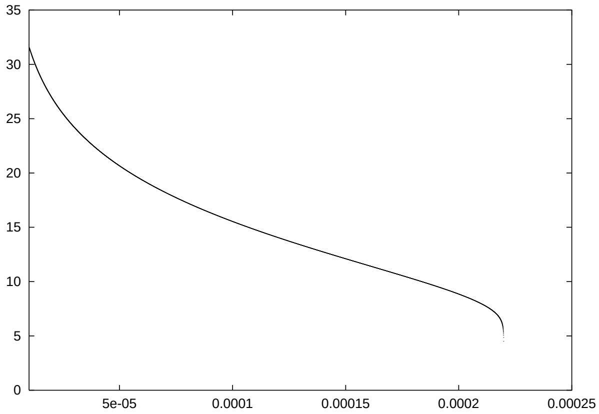

FIGURE 16. Plot of $\log(T(\rho_0))$ versus ρ_0

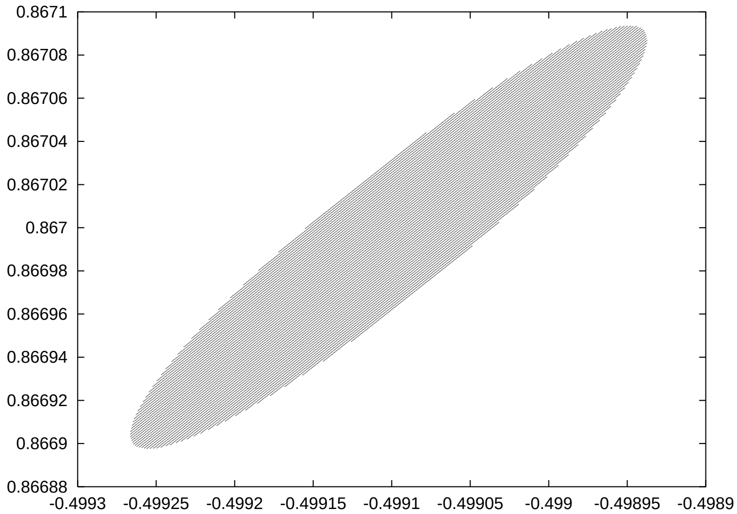

FIGURE 17. Region of effective stability around the point $t = 0$ of the periodic orbit replacing L_5. To compare this region with the one obtained in the normal form, we have used the same window as in Figure 14.

result obtained here is $\rho_0 = 1.9136 \times 10^{-4}$ and the maximal final radius is $\rho = 4.1835 \times 10^{-4}$. We note that the value of σ used in Section 5.4.3 is precisely the ratio ρ/ρ_0.

We can proceed as in Section 5.4.3 and plot the region of effective stability around the periodic orbit of L_5 in the (x, y)-plane of the RTBP space coordinates, see Figure 17.

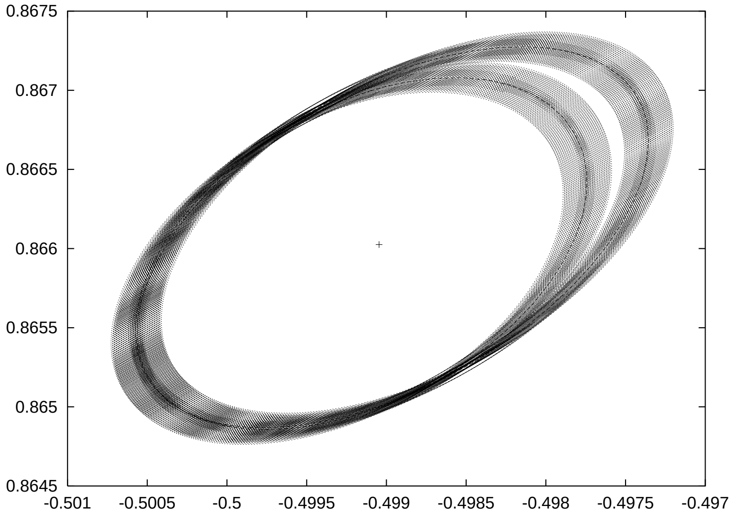

FIGURE 18. Region of effective stability around the periodic orbit replacing L_5. The triangular point is marked at the centre of the graphic.

7. CONCLUSIONS

In this paper we have developed a model for the motion of an asteroid under the gravitational attraction of Sun, Jupiter and Saturn. This model is based on computing, in suitable coordinates, a periodic orbit for these three bodies. Then, assuming that Sun, Jupiter and Saturn move on this orbit, it is not difficult to write the equations of motion for the asteroid; this is what we refer as BCCP. In suitable coordinates, the BCCP is a periodic time-dependent perturbation of the well known RTBP. In fact, the construction itself of the BCCP model is inspired in the construction of the RTBP model: while to construct the RTBP we use a circular periodic solution of the Sun-Jupiter system, for the BCCP we use a periodic, nearly circular, solution of the planar Sun-Jupiter-Saturn system.

Next, we perform a study of the dynamics around the triangular points. By means of a high order normal form calculation, it is possible to compute approximations to invariant tori (of dimensions 2, 3 and 4) nearby. Moreover, using suitable estimates on the remainder of this normal form, we can also derive a region such that the time needed to go away from it is bigger that the age of the Solar system. We have also used a second approach for the computation of these regions of effective stability: the computation of a suitable first integral. We have seen that the first integral produces a slightly larger region of stability but, on the other hand, it does not provide with a complete description of the dynamics inside this region as the normal form does. As we have used the same estimates for both approaches, it seems that first integrals are more suitable than normal forms for estimating practical stability regions, but normal forms give a complete description of the dynamics inside the region. If we compare the stability region here for $t = 0$ with previous results on the RTBP, we see that the region here (Figure 17) is smaller than that of the RTBP. This is an expected result since the BCCP is more complex and contains more resonances than the RTBP.

However, when we consider the time dependence, we have that the position in the physical space (by physical space we mean positions and velocities, without the time) of the region of effective stability depends (periodically) on time. Let us call $S(t) \subset \mathbb{R}^6$ to this region and, as the one obtained using the first integral is larger, we will focus on that one. Now, let us consider the region $S \subset \mathbb{R}^6$ of physical space "swept" by the regions $S(t)$, $S = \cup_t S(t)$. For instance, Figure 17 shows a section of $S(0)$, and Figure 18 shows a slice of S. If we denote by R the region of effective stability for the RTBP obtained in [10] we have that this region does not cover the region S: if we look at Figure 18, R is centred at the triangular point and S is following the periodic orbit leaving R in the middle. This means that the region S that we have obtained, although is smaller, is not contained in R. Unfortunately, there are no Trojan asteroids inside S, mainly due to the large component in the z direction (we recall Figures 5, 6 and 7).

Hence, the derivation of a computer assisted proof for the stability of the Trojan asteroids needs a methodology able to deal with motions far from equilibrium. This was one of the main goals of [34] but the application of those techniques to the BCCP model looks very difficult. This is actually work in progress.

Acknowledgements

The authors want to thank G. Gómez and C. Simó for their comments on a previous version of this manuscript. This research has been supported by the CICYT grant BFM2000–0623 and the CIRIT grant 2000SGR–00027.

References

[1] M.A. Andreu. *The quasi-bicircular problem*. PhD thesis, Univ. Barcelona, 1998.

[2] M.A. Andreu and C. Simó. The quasi-bicircular problem for the Earth-Moon-Sun parameters. Preprint, 2000.

[3] V.I. Arnold. Proof of A.N. Kolmogorov's theorem on the preservation of quasi-periodic motions under small perturbations of the Hamiltonian. *Russian Math. Surveys*, 18(5):9–36, 1963.

[4] V.I. Arnold. Instability of dynamical systems with several degrees of freedom. *Soviet Math. Dokl.*, 5:581–585, 1964.

[5] V.I. Arnold, V.V. Kozlov, and A.I. Neishtadt. *Dynamical Systems III*, volume 3 of *Encyclopaedia Math. Sci.* Springer, Berlin, 1988.

[6] G. Benettin, F. Fassò, and M. Guzzo. Nekhoroshev-stability of L_4 and L_5 in the spatial Restricted Three-Body Problem. *Regul. Chaotic Dyn.*, 3(3):56–72, 1998.

[7] E. Bowell. The asteroid orbital elements database. Project funded principally by NASA grant NAG5-4741, and in part by the Lowell Observatory endowment. For more information, visit the URL `http://www.naic.edu/~nolan/astorb.html`.

[8] H.W. Broer, G.B. Huitema, and M.B. Sevryuk. *Quasi-Periodic Motions in Families of Dynamical Systems: Order amidst Chaos*, volume 1645 of *Lecture Notes in Math.* Springer, New York, 1996.

[9] E. Castellà and À. Jorba. On the vertical families of two-dimensional tori near the triangular points of the Bicircular problem. *Celestial Mech.*, 76(1):35–54, 2000.

[10] A. Celletti and A. Giorgilli. On the stability of the Lagrangian points in the spatial Restricted Three Body Problem. *Celestial Mech.*, 50(1):31–58, 1991.

[11] V. Companys, G. Gómez, À. Jorba, J. Masdemont, J. Rodríguez, and C. Simó. Use of Earth-Moon libration points for future missions. In K.T. Alfriend, I.M. Ross, A.K. Misra, and C.F. Peters, editors, *AAS/AIAA Astrodynamics Conference*, volume 90 of *Advances in the Astronautical Sciences*, pages 1655–1666, San Diego, U.S.A., 1996. American Astronautical Society.

[12] J. Cronin, P.B. Richards, and L.H. Russell. Some periodic solutions of a four-body problem. *Icarus*, 3:423–428, 1964.

[13] J.M.A. Danby. Stability of the triangular points in the elliptic restricted problem of three bodies. *Astron. J.*, 69:165–172, 1964.

[14] A. Deprit and A. Deprit-Bartolome. Stability of the triangular Lagrangian points. *Astron. J.*, 75(2):173–179, 1967.

[15] C. Díez, À. Jorba, and C. Simó. A dynamical equivalent to the equilateral libration points of the real Earth-Moon system. *Celestial Mech.*, 50(1):13–29, 1991.

[16] R. Douady. Stabilité ou instabilité des points fixes elliptiques. *Ann. Sci. École Norm. Sup. (4)*, 21:1–46, 1988.

[17] E. Fontich and P. Martín. Arnold diffusion in perturbations of analytic integrable Hamiltonian systems. *Discrete Contin. Dynam. Systems*, 7(1):61–84, 2001.

[18] A. Giorgilli. Rigorous results on the power expansions for the integrals of a Hamiltonian system near an elliptic equilibrium point. *Ann. Inst. H. Poincaré Phys. Théor.*, 48(4):423–439, 1988.

[19] A. Giorgilli, A. Delshams, E. Fontich, L. Galgani, and C. Simó. Effective stability for a Hamiltonian system near an elliptic equilibrium point, with an application to the restricted three body problem. *J. Differential Equations*, 77:167–198, 1989.

[20] A. Giorgilli and L. Galgani. Formal integrals for an autonomous Hamiltonian system near an equilibrium point. *Celestial Mech.*, 17:267–280, 1978.

[21] A. Giorgilli and C. Skokos. On the stability of the Trojan asteroids. *Astron. Astrophys.*, 317:254–261, 1997.

[22] G. Gómez, À. Jorba, J. Masdemont, and C. Simó. Quasiperiodic orbits as a substitute of libration points in the solar system. In A.E. Roy, editor, *Predictability, Stability and Chaos in N-Body Dynamical Systems*, pages 433–438. Plenum Press, 1991.

[23] G. Gómez, À. Jorba, J. Masdemont, and C. Simó. A quasiperiodic solution as a substitute of l_4 in the Earth-Moon system. In *Proceedings of the 3rd International Sysmposium on Spacecraft Flight Dynamics*, pages 35–41, ESTEC, Noordwijk, Holand, 1991. ESA Publications Division.

[24] G. Gómez, À. Jorba, J. Masdemont, and C. Simó. Study of Poincaré maps for orbits near Lagrangian points. ESOC contract 9711/91/D/IM(SC), final report, European Space Agency, 1993.

[25] G. Gómez, J. Llibre, R. Martínez, and C. Simó. Station keeping of libration point orbits. ESOC contract 5648/83/D/JS(SC), final report, European Space Agency, 1985.

[26] G. Gómez, J. Masdemont, and J.M. Mondelo. Solar system models with a selected set of frequencies. Preprint, 2001.

[27] À. Jorba. A methodology for the numerical computation of normal forms, centre manifolds and first integrals of Hamiltonian systems. *Exp. Math.*, 8(2):155–195, 1999.

[28] À. Jorba. A numerical study on the existence of stable motions near the triangular points of the real Earth-Moon system. *Astron. Astrophys.*, 364(1):327–338, 2000.

[29] À. Jorba. On practical stability regions for the motion of a small particle close to the equilateral points of the real Earth–Moon system. Proceedings of the *III International Symposium HAMSYS-98. Geometrical Methods in Hamiltonian Systems and Celestial Mechanics.* Pátzcuaro (México), December 7–11, 1998. World Scientific (to appear), 2000.

[30] À. Jorba and C. Simó. Effective stability for periodically perturbed Hamiltonian systems. In J. Seimenis, editor, *Hamiltonian Mechanics: Integrability and Chaotic Behaviour*, volume 331 of *NATO Adv. Sci. Inst. Ser. B Phys.*, pages 245–252. Held in Toruń, Polland, 28 June–2 July 1993. Plenum, New York, 1994.

[31] À. Jorba and C. Simó. On quasiperiodic perturbations of elliptic equilibrium points. *SIAM J. Math. Anal.*, 27(6):1704–1737, 1996.

[32] À. Jorba and J. Villanueva. On the normal behaviour of partially elliptic lower dimensional tori of Hamiltonian systems. *Nonlinearity*, 10:783–822, 1997.

[33] À. Jorba and J. Villanueva. On the persistence of lower dimensional invariant tori under quasi-periodic perturbations. *J. Nonlinear Sci.*, 7:427–473, 1997.

[34] À. Jorba and J. Villanueva. Numerical computation of normal forms around some periodic orbits of the Restricted Three Body Problem. *Phys. D*, 114:197–229, 1998.

[35] À. Jorba and J. Villanueva. The fine geometry of the Cantor families of invariant tori in Hamiltonian systems. To appear in the Proceedings of the 3rd European Congress of Mathematics held in Barcelona, July 10th to 14th, 2000.

[36] `http://ssd.jpl.nasa.gov/horizons.html`.

[37] A.N. Kolmogorov. On the persistence of conditionally periodic motions under a small change of the Hamilton function. *Dokl. Acad. Nauk. SSSR*, 98(4):527–530, 1954.

[38] A.M. Leontovich. On the stability of the Lagrange periodic solutions of the restricted problem of three bodies. *Soviet Math. Dokl.*, 3:425–428, 1962.

[39] C. Marchal. The quasi integrals. *Celestial Mech.*, 21:183–191, 1980.

[40] C. Marchal. *The three-body problem*. Elsevier, 1990.

[41] A.P. Markeev. Stability of the triangular Lagrangian solutions of the restricted three-body problem in the three-dimensional circular case. *Soviet Astronom. AJ*, 15:682–686, 1971.

[42] A.P. Markeev. On the stability problem for the Lagrange solutions of the restricted three-body problem. *J. Appl. Math. Mech.*, 37:713–717, 1973.

[43] K. R. Meyer and G. R. Hall. *Introduction to Hamiltonian Dynamical Systems and the N-Body Problem*. Springer, New York, 1992.

[44] K. R. Meyer and D. S. Schmidt. The stability of the Lagrange triangular point and a theorem of Arnold. *J. Differential Equations*, 62(2):222–236, 1986.

[45] J. Moser. On invariant curves of area-preserving mappings of an annulus. *Nachr. Akad. Wiss. Göttingen Math.-Phys. Kl. II*, 2:1–20, 1962.

[46] N.N. Nekhoroshev. An exponential estimate of the time of stability of nearly-integrable Hamiltonian systems. *Russian Math. Surveys*, 32:1–65, 1977.

[47] L. Niederman. Stability over exponentially long times in the planetary problem. *Nonlinearity*, 9(1):1703–1751, 1996.

[48] C. Simó. Estabilitat de sistemes Hamiltonians. *Mem. Real Acad. Cienc. Artes Barcelona*, 48(7):303–348, 1989.

[49] C. Simó, G. Gómez, À. Jorba, and J. Masdemont. The Bicircular model near the triangular libration points of the RTBP. In A.E. Roy and B.A. Steves, editors, *From Newton to Chaos*, pages 343–370, New York, 1995. Plenum Press.

[50] V. Szebehely. *Theory of Orbits*. Academic Press, 1967.